

See discussions, stats, and author profiles for this publication at: <https://www.researchgate.net/publication/51167661>

Anticancer Properties of an Important Drug Lead Podophyllotoxin Can Be Efficiently Mimicked by Diverse Heterocyclic Scaffolds Accessible via One-Step Synthesis

ARTICLE in JOURNAL OF MEDICINAL CHEMISTRY · JUNE 2011

Impact Factor: 5.45 · DOI: 10.1021/jm200410r · Source: PubMed

CITATIONS

24

READS

67

18 AUTHORS, INCLUDING:



Igor V Magedov

New Mexico Institute of Mining and Technology

33 PUBLICATIONS 805 CITATIONS

SEE PROFILE



Madhuri Manpadi

Drury University

24 PUBLICATIONS 469 CITATIONS

SEE PROFILE



Steffen Renner

Novartis

42 PUBLICATIONS 1,277 CITATIONS

SEE PROFILE



Snezna Rogelj

New Mexico Institute of Mining and Technology

60 PUBLICATIONS 4,325 CITATIONS

SEE PROFILE

Published in final edited form as:

J Med Chem. 2011 June 23; 54(12): 4234–4246. doi:10.1021/jm200410r.

Anticancer Properties of an Important Drug Lead Podophyllotoxin Can Be Efficiently Mimicked by Diverse Heterocyclic Scaffolds Accessible via One-Step Synthesis

Igor V. Magedov^{†,*}, Liliya Frolova[†], Madhuri Manpadi[†], Uma devi Bhoga[‡], Hong Tang[§], Nikolai M. Evdokimov[†], Olivia George[#], Kathy Hadje Georgiou[‡], Steffen Renner^Σ, Matthäus Getlic^Π, Tiffany L. Kinnibrugh[†], Manuel A. Fernandes[‡], Severine Van slambrouck[†], Wim F. A. Steelant^{†,‡}, Charles B. Shuster[#], Snezna Rogelj[§], Willem A. L. van Otterlo^{‡,∞,*}, and Alexander Kornienko^{†,*}

Departments of Chemistry and Biology, New Mexico Institute of Mining and Technology, Socorro, New Mexico 87801, USA; Molecular Sciences Institute, School of Chemistry, University of the Witwatersrand, PO Wits, 2050 Johannesburg, South Africa; Department of Biology, New Mexico State University, Las Cruces, New Mexico 88003; Max Planck Institute for Molecular Physiology, Dortmund, Germany; Chemical Genomics Centre of the Max Planck Society, Dortmund, Germany; Department of Chemistry and Polymer Sciences, Stellenbosch University, Stellenbosch, Western Cape South Africa

Abstract

Structural simplification of an antimitotic natural product podophyllotoxin with mimetic heterocyclic scaffolds constructed using multicomponent reactions led to the identification of compounds exhibiting low nanomolar antiproliferative and apoptosis-inducing properties. The most potent compounds were found in the dihydropyridopyrazole, dihydropyridonaphthalene, dihydropyridindole and dihydropyridopyrimidine scaffold series. Biochemical mechanistic studies performed with dihydropyridopyrazole compounds showed that these heterocycles inhibit *in vitro* tubulin polymerization and disrupt the formation of mitotic spindles in dividing cells at low nanomolar concentrations, in a manner similar to podophyllotoxin itself. Separation of a racemic dihydropyridonaphthalene into individual enantiomers demonstrated that only the optical antipode matching the absolute configuration of podophyllotoxin possessed potent anticancer activity. Computer modeling, performed using the podophyllotoxin binding site on beta-tubulin, provided a theoretical understanding of these successful experimental findings.

*Corresponding authors. Tel.: +1 575 835 6886; fax: +1 575 835 5364; imagedov@nmt.edu. Tel.: +27 21 808 3344; fax: +27 21 808 3360; wvo@sun.ac.za. Tel.: +1 575 835 5884; fax: +1 575 835 5364; akornien@nmt.edu.

[†]Department of Chemistry, New Mexico Institute of Mining and Technology

[‡]Molecular Sciences Institute, School of Chemistry, University of the Witwatersrand

[§]Department of Biology, New Mexico Institute of Mining and Technology

[#]New Mexico State University

^ΣMax Planck Institute for Molecular Physiology, Dortmund

^ΠChemical Genomics Centre of the Max Planck Society, Dortmund

[∞]Department of Chemistry and Polymer Sciences, Stellenbosch University

[‡]Present address: School of Science, Technology and Engineering Management, St. Thomas University, 16401 NW 37th Avenue, Miami Gardens, FL 33054, USA

Supporting Information Available: an enlarged representation of Figure 4, details of the computational work, chiral HPLC and copies of ¹H and ¹³C NMR spectra of all new compounds. This material is available free of charge via the Internet at <http://pubs.acs.org>.

Introduction

Natural products are often referred to as evolutionarily selected “privileged structures” that are likely to manifest multiple biological activities.¹ Because of their intrinsic biorelevance they have historically been a major source of new pharmaceuticals. For example, in the area of cancer, the fraction of drugs derived from natural products amounts to 60% and hit rates obtained by screening of natural product-derived collections of compounds are dramatically higher than those resulting from high throughput screens of combinatorial libraries.^{2,3} However, the structures of natural products are generally quite complex, incorporating intricate ring systems and large numbers of stereogenic centers. Therefore, preparations of natural product-based libraries inevitably involve rather sophisticated and laborious synthetic sequences. Furthermore, therapeutic development of promising leads resulting from these libraries is significantly impeded by the problem of large-scale compound supply. These challenges are becoming increasingly more relevant due to the renewed interest in natural products by the pharmaceutical industry and to the failure of alternative methods to deliver many therapeutic lead compounds.⁴

In a search for general solutions to the above-mentioned problems, we have initiated a research program aimed at structural simplification of bioactive natural products by designing mimetic scaffolds that can be constructed using one-step multicomponent reactions (MCRs).⁵ We recently described a dihydropyridopyrazole scaffold designed on the basis of a potent anticancer cyclolignan, podophyllotoxin, and readily prepared by combining an aminopyrazole, tetronic acid and an aromatic or heteroaromatic aldehyde in a one-pot condensation process (Figure 1).^{5a,b}

The utilization of podophyllotoxin as a lead in anticancer drug design has resulted in useful cancer fighting drugs such as etoposide, teniposide and etoposide phosphate.⁶ These successes have fueled further research efforts in this area directed at the preparation of analogues, which are expected to have improved potency and reduced toxicity. Unfortunately, the complex chemical structure of podophyllotoxin virtually prevents the generation of its analogues from simple commercially available materials and, therefore, derivatization of podophyllotoxin has been the main strategy to obtain structure-activity relationship (SAR) information.⁷ This SAR has often not been systematic and has been limited by the type of chemistry that podophyllotoxin can undergo. As a result many designed analogues are synthetically inaccessible from the parent natural product. For example, modifications of ring E are extremely difficult due to the presence of the three methoxy groups in the starting lignan. To achieve useful modifications of ring E, one therefore needs to resort to total synthesis efforts. Indeed, Berkowitz and co-workers achieved a total synthesis of the 3',4',5'-tridemethoxy analogue of podophyllotoxin (ring E = Ph), which is inaccessible by derivatization of the natural product itself.⁸ However, the length of the synthetic route, which involved 19 steps from commercially available materials, serves to illustrate the challenge a medicinal chemist would face following such a strategy. The versatility of the MCR approach, however, has allowed us to prepare a diverse library of podophyllotoxin mimetics and generate systematic SAR data. Thus, the utilization of requisite aldehyde starting materials leads directly to the desired modification of ring E (Figure 1). Furthermore, the use of various aromatic and heteroaromatic amines in lieu of the aminopyrazole component has allowed us to expand the scope of possible A,B-ring system substitutions in these podophyllotoxin-mimetic scaffolds. Such SAR-guided structure optimization work, along with biochemical mechanistic investigations, have led to several important breakthroughs in this area of research. Firstly, we were able to significantly enhance the potency and identify compounds that rival podophyllotoxin in antiproliferative and apoptosis-inducing properties. Secondly, we obtained strong evidence that the dihydropyridopyrazoles retain the antitubulin mode of action of the natural

cyclolignan, attesting to the *bona fide* mimicry of the podophyllotoxin's structure by this heterocyclic scaffold. Thirdly, we found that nanomolar antiproliferative potencies are not limited to compounds based on the dihydropyridopyrazole scaffold, but also reside with dihydropyridonaphthalene, dihydropyridoindole and dihydropyridopyrimidine mimetic libraries, pointing to the possibility of scaffold modification as an additional option in the pursuit of a tubulin-targeting clinically useful anticancer agent. Finally, computational studies revealed a structural basis for these successful findings and further supported the theoretical framework of the approach. Altogether, the results of this study present a strong case for establishing the mimetic scaffold approach as a useful paradigm in drug discovery.

Results and Discussion

Optimized dihydropyridopyrazoles rival podophyllotoxin in antiproliferative effect

Because the A,B-ring system in podophyllotoxin is sterically more demanding and less polar than the pyrazole ring, we initially expected that some degree of substitution of the pyrazole moiety would be required for activity and focused on the C-3 Me-substituted compounds ($R^1=Me$, $R^2=H$, Figure 1).^{5a,b} Further work revealed, however, that low nanomolar potencies are predominantly associated with compounds containing the unsubstituted pyrazole moiety ($R=H$, Table 1). Synthesis of such compounds involved combining 5-aminopyrazole, tetronic acid and an aromatic aldehyde in ethanol and refluxing these reaction mixtures for 0.5–3 hours. The desired dihydropyridopyrazoles precipitated upon cooling to room temperature. In addition, in most cases the products were analytically pure without any further purification. Evaluation of these heterocycles for antiproliferative activity was performed using HeLa and MCF-7 cancer cell lines as models for human cervical and breast adenocarcinomas, respectively (Table 1). While the structural requirements of ring E in podophyllotoxin have seen little investigation (due to the synthetically unsurmountable challenge of removing or replacing the methoxy groups), our data show that in the dihydropyridopyrazole series the methoxy substituents are not important and the combination of 3-bromo with 2-hydroxy substitution brings about the highest potencies. Thus, the progressive replacement of the methoxy groups with meta-bromo substitution (**2**→**4**→**6**→**10**) and the subsequent addition of a 2-hydroxy group (**12**, **14** and **16**) led to compounds with low nanomolar potencies. Of particular note was that the 3,5-dibromo-2-hydroxy compound (**16**) is equipotent to podophyllotoxin with GI_{50} values of 20 and 10 nM against HeLa and MCF-7 cells, respectively.

Optimized dihydropyridopyrazoles rival podophyllotoxin in apoptosis-inducing effect

Because the anticancer efficacy of many current chemotherapeutic agents is strongly correlated with their ability to induce apoptosis in cancer cells,⁹ we compared the apoptosis-inducing potential of the potent dihydropyridopyrazoles with that of podophyllotoxin. This was accomplished by performing caspase-3 activation¹⁰ and flow cytometric Annexin-V/propidium iodide¹¹ assays, two common methods used to detect and quantify such hallmarks of the apoptotic process as caspase cascade activation and the appearance of the phosphatidylserine lipid in the outer leaflet of the cellular membrane (Figure 2). These assays, carried out with Jurkat cells (a model for T-cell leukemia), revealed that both podophyllotoxin and the 3,5-dibromo analogues **10** and **16** exhibit similar magnitudes of apoptosis induction at high nanomolar concentrations (Figure 2A). In addition, similar to podophyllotoxin, the induction of apoptosis by **16** occurs at concentrations as low as 5–8 nM (Figure 2B), an observation that is consistent with the beneficial effect of the 2-hydroxy substituent in combination with the 3,5-dibromo substitution in ring E.

Dihydropyridopyrazoles retain anti-tubulin mode of action of podophyllotoxin

Using flow cytometric cell cycle analysis, we obtained evidence pointing to the retention of the antitubulin mechanism of action by the dihydropyridopyrazoles. Agents interfering with tubulin dynamics are known to arrest cells in M phase of the cell cycle.¹² Thus, similar to that of antimitotic podophyllotoxin, these compounds cause the accumulation of Jurkat cell populations with a 4N DNA content (data not shown). To confirm the retention of microtubule-destabilizing activity *in vitro*, a fluorimetry-based microtubule polymerization assay was employed.¹³ While taxol exhibited enhancement of microtubule formation relative to the effect of the DMSO control (Figure 3), library members **10** and **16** displayed a potent microtubule destabilizing effect in a manner similar to the tubulin polymerization inhibitor podophyllotoxin.

Similarly, examination of cultured HeLa cervical human cells treated with the dihydropyridopyrazoles revealed potent microtubule destabilizing activities. Analogue **16** disrupted both interphase- and mitotic microtubule organization at concentrations as low as 5 nM. As shown in Figure 4A (panel f), microtubules nucleating from the spindle poles are visible, but at 10 nM (panel g), virtually all microtubule nucleation from either spindle poles or kinetochores is ablated. In comparison, colchicine displayed no visible defect in microtubule organization at 5 nM (Figure 4B, panels j and n), whereas positive control podophyllotoxin caused similar effects on mitotic spindle formation (panel o) with no effect on interphase microtubule organization (panel k).

Further scaffold modifications lead to compounds possessing single-digit nanomolar antiproliferative potencies

In an attempt to expand the range of possible A,B-ring system substitutions in these podophyllotoxin-mimetic scaffolds we explored the use of various aromatic and heteroaromatic amines in lieu of the aminopyrazole component in the MCR process. The MCR literature contains a number of examples of cyclocondensation of aromatic amines with aldehydes and 1,3-dicarbonyl compounds. Importantly, as this work was in progress, scientists at Bayer CropScience AG utilized diversely substituted anilines in this process and prepared over 140 such heterolignans for their potential use as anti-insecticidal agents.^{14a} Furthermore, an MCR involving naphthyl amines, 1,3-dicarbonyl compounds and aldehydes had also been previously investigated by other researchers.¹⁵ Prompted by these successful literature examples, as well as by the results of computational docking studies (*vide infra*) which indicated that large hydrophobic residues in lieu of the A,B-ring system in podophyllotoxin could be accommodated at the binding site on β -tubulin, we investigated the reaction of α -naphthyl amine with tetrone acid and diversely substituted benzaldehydes (Figure 5, Table 2). The MCR was found to be as practical as that involving aminopyrazoles and the desired pentacycles precipitated from the refluxing ethanol solutions. However, the reaction yields were somewhat eroded, possibly by a number of competing side-reactions. Thus, the desired pentacycle **B** can further react with the Knoevenagel intermediate **A** at the second nucleophilic position of the nitrogen-bearing aromatic ring to give side product **C** (Figure 5), an outcome consistent with the experimental findings of Frackenpohl *et al.*^{14a} In addition, further slight reduction in reaction yields was observed in the case of 7-hydroxy- α -naphthylamine. It is likely that the presence of the naphtholic hydroxyl leads to side products **D**, as naphthols have been shown to be substrates for such MCR processes.¹⁶

The evaluation of these compounds for antiproliferative activity against HeLa and MCF-7 cells indicated that they are more potent than podophyllotoxin itself and many of them have GI₅₀ values as low as 3 nM (Table 2). The addition of a hydroxyl group to the naphtholic moiety had a beneficial effect by further lowering the GI₅₀ values, which is an excellent

finding considering the potential water solubility problems associated with these hydrophobic compounds.

Interestingly, the benefit of the 3-bromo substitution pattern in ring E, which was important in the case of the pyrazole-based scaffold (*vide supra*, Table 1), is absent in these naphthalene-fused pentacycles. In fact, the low nanomolar potencies were found for all 3-bromo-substituted ring E containing compounds (**19–25** and **27–33**), as well as the 3,4,5-trimethoxy-substituted ones (**18** and **26**). Therefore, in our further A,B-ring system modification efforts we limited the variations in the ring E moiety to just two, namely the 3,4,5-trimethoxy and 3,5-dibromo substitution patterns (Table 3).

Repositioning of the hydroxyl group in the starting α -naphthylamine from C-7 to C-9 (Table 3, entry 1) did not affect the successful outcome of the MCR process, which produced pentacycles **34** and **35**. Both compounds were found to have excellent antiproliferative potencies. However, the utilization of electron-rich naphthalene-1,4-diamine (entry 2) resulted in MCR products susceptible to aerial oxidation. While pentacycle **37** was synthesized in respectable yield and found to have excellent antiproliferative properties, compound **36** was too unstable for its chemical characterization and biological testing. Interestingly, the use of β -naphthylamine (entry 3) in the MCR process yields compounds **38** and **39**, in which the polycyclic scaffold is bent in the opposite direction compared with analogues **18–37**. As would be expected, the electrophilic attack by the Knoevenagel intermediate occurs preferentially at the α position of the naphthalene system. In contrast, in the tetrahydro system (entry 4), where the steric factors become more important than the electronic ones, the electrophilic attack occurs at the β' position and linear polycycles **40** and **41** are obtained exclusively. These regiochemical assignments are consistent with the NMR data and confirmed by X-ray structure determinations of select analogues.¹⁷ The biological testing of analogues **38–41** revealed that such a change in topology of the polycyclic scaffold has a strong effect on the antiproliferative potencies, raising the GI₅₀ values by about two orders of magnitude (compare **18** and **38** in Tables 2 and 3). Lastly, the previously unknown MCR processes utilizing heterocyclic amines, such as aminoindole, aminopyrazolone and aminopyrimidine, were performed and polycycles **42–47** were obtained in respectable yields (entries 5–7). Of these, the indole- and pyrimidine-containing analogues **42**, **43** and **46**, **47** exhibited nanomolar antiproliferative potencies. Overall, these experiments argue convincingly that nanomolar antiproliferative potencies can be achieved with a judicious choice of an A,B-ring system in the podophyllotoxin-mimetic libraries and highlight the scaffold modification as an additional resource in the pursuit of a tubulin-targeting clinically useful anticancer agent.

Ring E in podophyllotoxin mimetics is positioned quasixially with respect to the rest of the heterocyclic scaffold

To gain insight into the possible causes of the efficient mimicry of podophyllotoxin by these heterocyclic compounds, we performed density functional theory (DFT) conformational optimizations using the dihydropyridopyrazole scaffold. It is well-established that the quasixial positioning of ring E with respect to the rest of the molecule (rings A, B, C, and D) of podophyllotoxin is a key requirement for both efficient binding to the colchicine site on β -tubulin and the resulting antimitotic activity in this series of compounds.^{7a} For example, dehydropodophyllotoxin containing the aromatic ring C is totally inactive, while picropodophyllin, epimeric at C-2 (see Figure 1 for position numbering) and containing the cis-lactone moiety, has a significantly diminished activity. Both of these substances lack the axial orientation of ring E.¹⁸ Our computational results reveal that the dihedral angle of ring E with respect to the ABCD ring system in dihydropyridopyrazole **1** (124°, Figure 6B) is close to that of deoxypodophyllotoxin (116°, Figure 6A), confirming the quasixial

positioning of ring E in the dihydropyridopyrazole scaffold. In contrast, in deoxypicropodophyllin ring E occupies an equatorial position (144°, Figure 6C).

Potent MCR library members dock well to the podophyllotoxin binding site on β -tubulin

Based on our design hypothesis, the novel tubulin inhibitors were assumed to have comparable binding modes in the tubulin colchicine binding site when compared to the design template podophyllotoxin. Computational docking simulations were thus used to further investigate the validity of our design hypothesis. Several of the synthesized molecules were docked into the tubulin–podophyllotoxin crystal structure from Knossow and co-workers¹⁹ (PDB code 1SA1). Despite a fairly low resolution of 4.2 Å and the absence of well defined hydrogen bonds between podophyllotoxin and tubulin in the crystal structure, we were able to reproduce the observed binding mode of podophyllotoxin with good accuracy (RMSD = 0.936), as has also been reported by other groups.^{20a,21}

Two major observations were made in the docking results. Firstly, docking of the *R*-enantiomers of the compounds resulted in a comparable binding mode relative to podophyllotoxin, whereas the *S*-enantiomers led to an alternate binding mode with the ring systems flipped by 180° (*vide infra*). Secondly, we found that the most potent compounds, having additional rings added in a nonlinear bent arrangement relative to podophyllotoxin (e.g. **18–33**), were predicted to bind in a slightly twisted conformation, maximizing the overlap of the ring systems of our inhibitors with the ring system of podophyllotoxin (see the binding mode of *R*-**19** in Figure 7a). More interesting, this twisted orientation of the rings was still maintained in the tricycles that did not have additional rings, and that did not have additional methyl groups on the B ring (see *R*-**16** in Figure 7b). If the methyl was present, a different binding mode with a twist into the opposite direction (as compared to podophyllotoxin) was observed (see *R*-**5** in Figure 7c). This may explain the observed weakening effect of the B ring methyl group on the biological potency, as for example found with pyrazoles *R*-**5** and *R*-**6**, the former only differing by the extra methyl group, but being significantly less potent than *R*-**6**. According to the docking study the additional methyl would clash with the protein and prevent the preferred binding mode. Other ligands with groups protruding into the same direction, like **38** and **39**, that have an additional ring occupying the same space as the pyrazole methyl group, and compounds **44**, **45**, having a carbonyl group pointing into this direction, were also found to be significantly less potent when compared to similar ligands without these groups.

Of interest was that the SAR on the E ring appeared not to be explained by the docking simulations. Most different ring E variants docked well into the binding site and showed comparable docking scores, supporting the notion that the site occupied by this ring is dominated by hydrophobic interactions and allows for promiscuous occupancy by various functional groups on the E ring. This supports the data in Table 2 which show very little fluctuation in the bioactivities of the compound sets **18–25** and **26–33**, these compounds only differing in the substitution of the E ring.

Only the enantiomer matching the absolute configuration of podophyllotoxin shows potent anticancer activity and good docking properties

Importantly, the modeling study led to the observation that the stereochemical arrangement at carbon C-1 (podophyllotoxin numbering, Figure 1) was critical to the ability of the MCR products to overlap with the podophyllotoxin ligand. The docking results showed that compounds with the “wrong” configuration, relative to the *R* configuration of podophyllotoxin, did not dock well at all – in fact a “flip” of the BCD or ABCD core of the MCR product was often required to afford a satisfactory fit. For example, Figure 7 depicts the best docking fit of *R*-**19** (Figure 7a) and *S*-**19** (Figure 7d), respectively. *R*-**19** nicely

overlaps with podophyllotoxin (Figure 7a), while *S*-**19** shows a very poor overlay with the natural product (Figure 7d); of significance is that the modeling predicted the majority of the “best fits” for this molecule to require a “flip” of the compound in the binding site as shown in the figure 7d.

Next, we investigated if this predicted difference in docking propensity would translate into an actual difference in the bioactivities of the different enantiomers. To this end, compound **19** was chosen for closer examination, as the naphthalene moiety and two bromine atoms were expected to assist in the subsequent single crystal X-ray diffraction studies. A sample of **19** was therefore separated into its enantiomers *R*-**19** and *S*-**19** by chiral HPLC (see supplementary information). Subsequent biochemical evaluation of the two compounds confirmed that one optical antipode was indeed much more potent (see Figure 8). A larger scale HPLC separation then gave in hand sufficient amounts of *R*-**19** and *S*-**19**, such that crystals could be obtained for the less potent enantiomer. These were then duly analyzed by X-ray crystallography to confirm that this antipode had the *S* stereochemistry (Figure 8). These results further support the favored binding of the *R*-MCR derivatives to the active site of tubulin, which is responsible for the higher potency observed for the *R*-enantiomer. Furthermore, this corroborated the hypothesis that our compounds, synthesized in a single step, were interacting with tubulin in a similar manner to podophyllotoxin.

Conclusions

In summary, notwithstanding their significantly simpler structures, several heterocyclic podophyllotoxin-mimetic libraries rival the parent natural product by exhibiting nanomolar antiproliferative activities against human cancer cells and manifesting potent apoptosis inducing properties. At present such libraries include compounds based on dihydropyridopyrazole, dihydropyridonaphthalene, dihydropyridoindole and dihydropyridopyrimidine scaffolds. These promising discoveries, as well as the computer modeling results, together indicate that potent activities may be found in many related, but yet unexplored, podophyllotoxin-mimetic heterocycles that can be prepared using the MCR process described in this investigation. Importantly, using the dihydropyridopyrazole compounds we demonstrated that, in a manner similar to podophyllotoxin, these heterocycles inhibit *in vitro* tubulin polymerization and disrupt the formation of mitotic spindle in dividing cells at low nanomolar concentrations, thus attesting to their *bona fide* mimicry of podophyllotoxin. This is further corroborated by separation of a potent racemic dihydropyridonaphthalene compound into individual enantiomers and demonstration of high potency associated only with the enantiomer matching the absolute configuration of podophyllotoxin, an outcome predicted by computer modeling. Altogether, the results of this study present a strong case for the utilization of a mimetic scaffold approach as a useful paradigm in drug discovery.

Experimental Section

General Synthetic Methods

All aldehydes, aminopyrazoles, ethanol and tetronic acid were purchased from commercial sources and used without purification. Triethylamine (Et₃N) was distilled from CaH₂. All reactions were performed in a reaction vessel open to the atmosphere and monitored by thin layer chromatography (TLC) on pre-coated (250 μm) silica gel 60F₂₅₄ glass-backed plates. Visualization was accomplished with UV light and aqueous ceric ammonium molybdate solution or potassium permanganate stain followed by charring on a hot-plate. Flash column chromatography was performed on silica gel (32–63 μm, 60 Å pore size). ¹H and ¹³C NMR spectra were recorded on Jeol Eclipse 300 or Bruker Avance III 400 spectrometers. Chemical shifts (δ) are reported in ppm relative to the TMS internal standard. Abbreviations

are as follows: s (singlet), d (doublet), dd (doublet of doublets), t (triplet), q (quartet), m (multiplet). HRMS analyses were performed at the Mass Spectrometry Facility, University of New Mexico. Samples were run on LCT Premier TOF mass spec. The synthesized compounds are at least 95% pure according to HPLC analysis.

General Procedure for Dihydropyridopyrazole Synthesis

A mixture of 5-aminopyrazole or 5-amino-3-methylpyrazole (1 mmol), tetronic acid (1 mmol), triethylamine (0.05 mL), and a corresponding aldehyde (1 mmol) in EtOH (4 mL) was refluxed for 0.5–3 h. The reaction mixture was allowed to cool to rt, and the precipitated product was collected by vacuum filtration and washed with EtOH (3 mL) at rt. In most cases, the products were >98% pure as judged by NMR analysis. When an impurity was present, the product was recrystallized from DMF/H₂O.

4-(3,4,5-Trimethoxyphenyl)-1,4,7,8-tetrahydro-5H-furo[3,4-b]pyrazolo[4,3-e]pyridin-5-one (2)

75% as white solid, mp = 262–263 °C. ¹H NMR (DMSO-*d*₆) δ: 3.79 (s, 9H), 4.85–5.00 (dd, *J*=15Hz, 2H), 4.92 (s, 1H), 6.48 (s, 2H), 7.40 (s, 1H), 10.21 (s, 1H), 12.18 (s, 1H); ¹³C NMR (DMSO-*d*₆) δ 172.6, 160.6, 153.1, 147.8, 141.5, 136.6, 136.4, 105.5, 102.8, 96.0, 60.5, 56.4, 56.3; HRMS *m/z* (ESI) calcd for C₁₇H₁₈N₃O₅ (M + H)⁺ 344.1246, found 344.1238.

4-(3-Bromo-4,5-dimethoxyphenyl)-1,4,7,8-tetrahydro-5H-furo[3,4-b]pyrazolo[4,3-e]pyridin-5-one (4)

72% as white solid, mp = 244–246 °C. ¹H NMR (DMSO-*d*₆) δ: 3.67 (s, 3H, OCH₃), 3.79 (s, 3H, OCH₃), 4.80–5.11 (m, 3H, CH + CH₂), 6.82 (s, 1H, CH_{Ar}), 6.98 (s, 1H, CH_{Ar}), 7.40 (s, 1H, CH_{pyr}), 10.27 (s, 1H, NH), 12.24 (s, 1H, NH); ¹³C NMR (DMSO-*d*₆) δ 172.6 (C=O), 161.2 (C_{Ar}), 153.7 (C_{Ar}), 144.7 (C_{Ar}), 144.0 (C_{Ar}), 122.9 (C_{Ar}), 116.9 (C_{Ar}), 112.6 (C_{Ar}), 112.5 (C_{Ar}), 105.5 (C_{pyr}), 95.2 (C=C-NH), 65.6 (OCH₂), 60.5 (OCH₃), 56.6 (OCH₃), 34.5 (CH); HRMS *m/z* (ESI) calcd for C₁₆H₁₄BrN₃O₄Na (M + Na)⁺ 414.0065, found 414.0058.

4-(3-Bromophenyl)-1,4,7,8-tetrahydro-5H-furo[3,4-b]pyrazolo[4,3-e]pyridin-5-one (6)

71% as white solid, mp = 294–296 °C. ¹H NMR (DMSO-*d*₆) δ: 4.81–5.01 (m, 3H), 7.23 (s, 1H), 7.35 (s, 4H), 10.29 (s, 1H), 12.25 (s, 1H); ¹³C NMR (DMSO-*d*₆) δ 172.4, 161.1, 149.2, 130.9, 130.5, 130.4, 129.6, 121.4, 105.5, 95.3, 65.6, 35.6; HRMS *m/z* (ESI) calcd for C₁₄H₁₀BrN₃O₂Na (M + Na)⁺, 353.9854, found 353.9859.

4-(5-bromo-3-pyridinyl)-3-methyl-1,4,7,8-tetrahydro-5H-furo[3,4-b]pyrazolo[4,3-e]pyridin-5-one (7)

88% as white solid, mp = >300 °C. ¹H NMR (DMSO-*d*₆) δ: 1.78 (s, 3H), 4.84–4.93 (dd, *J*=15Hz, 2H), 4.98 (s, 1H), 7.77 (d, *J* = 1.9 Hz, 1H), 8.46 (d, *J* = 1.9 Hz, 1H), 8.52 (d, 1H, *J* = 1.9 Hz), 10.28 (s, 1H), 12.04 (s, 1H); ¹³C NMR (DMSO-*d*₆) δ 172.9, 161.4, 149.4, 147.7, 143.2, 137.9, 121.5, 101.1, 94.9, 65.6, 32.3, 10.2; HRMS *m/z* (ESI) calcd for C₁₄H₁₁BrN₄O₂Na (M + Na)⁺ 368.9963, found 368.9963.

4-(5-Bromo-3-pyridinyl)-1,4,7,8-tetrahydro-5H-furo[3,4-b]pyrazolo[4,3-e]pyridin-5-one (8)

76% as white solid, mp = 283–284 °C. ¹H NMR (DMSO-*d*₆) δ: 4.80–5.02 (m, 3H), 5.02 (s, 1H), 7.37 (s, 1H), 7.73 (s, 1H), 8.43 (s, 1H), 8.47 (s, 1H), 10.33 (s, 1H), 12.28 (s, 1H); ¹³C NMR (DMSO-*d*₆) δ 172.9, 161.6, 149.4, 147.6, 143.6, 138.3, 129.4, 120.9, 104.1, 93.9, 65.5, 32.2; HRMS *m/z* (ESI) calcd for C₁₂H₉BrN₄O₂Na (M + Na)⁺ 354.9807, found 354.9807.

4-(3,5-Dibromophenyl)-3-methyl-1,4,7,8-tetrahydro-5H-furo[3,4-b]pyrazolo[4,3-e] pyridin-5-one (9)

85% as white solid, mp = 290–292 °C. ^1H NMR (DMSO- d_6) δ : 1.89 (s, 3H), 4.80–5.02 (m, 3H), 7.39 (s, 2H), 7.64 (s, 1H), 10.28 (s, 1H), 12.04 (s, 1H); ^{13}C NMR (DMSO- d_6) δ 172.5, 161.1, 150.3, 147.4, 137.0, 130.2, 122.8, 101.9, 95.1, 65.4, 34.5, 10.2; HRMS m/z (ESI) calcd for $\text{C}_{15}\text{H}_{11}\text{Br}_2\text{N}_3\text{O}_2\text{Na}$ ($\text{M} + \text{Na}$) $^+$ 445.9116, found 445.9109.

4-(3,5-Dibromophenyl)-1,4,7,8-tetrahydro-5H-furo[3,4-b]pyrazolo[4,3-e]pyridin-5-one (10)

83% as white solid, mp = 268–270 °C. ^1H NMR (DMSO- d_6) δ : 4.82–5.06 (m, 3H), 7.38 (s, 3H), 7.62 (s, 1H), 10.36 (s, 1H), 12.29 (s, 1H); ^{13}C NMR (DMSO- d_6) δ 172.7, 161.7, 151.5, 147.2, 130.4, 122.9, 104.4, 95.2, 65.5, 34.6; HRMS m/z (ESI) calcd for $\text{C}_{14}\text{H}_9\text{Br}_2\text{N}_3\text{O}_2\text{Na}$ ($\text{M} + \text{Na}$) $^+$ 431.8959, found 431.8952.

4-(5-Bromo-2-hydroxy-3-methoxyphenyl)-3-methyl-1,4,7,8-tetrahydro-5H-furo[3,4-b]pyrazolo[4,3-e]pyridin-5-one (11)

85% as yellow solid, mp = 255–256 °C. ^1H NMR (DMSO- d_6) δ : 1.85 (s, 3H), 3.80 (s, 3H), 4.77–4.95 (dd, $J=15\text{Hz}$, 2H), 5.20 (s, 1H), 6.57 (s, 1H), 6.89 (s, 1H), 8.96 (s, 1H), 10.09 (s, 1H), 11.85 (s, 1H); ^{13}C NMR (DMSO- d_6) δ 172.3, 161.7, 148.9, 143.1, 136.9, 124.1, 113.0, 110.4, 103.3, 95.7, 56.8, 31.1, 10.3; HRMS m/z (ESI) calcd for $\text{C}_{16}\text{H}_{14}\text{BrN}_3\text{O}_4\text{Na}$ ($\text{M} + \text{Na}$) $^+$ 414.0065, found 414.0051.

4-(5-Bromo-2-hydroxy-3-methoxyphenyl)-1,4,7,8-tetrahydro-5H-furo[3,4-b]pyrazolo [4,3-e]pyridin-5-one (12)

81% as pink solid, mp = 248–250 °C. ^1H NMR (DMSO- d_6) δ : 3.79 (s, 3H), 4.82–5.04 (dd, $J=15\text{Hz}$, 2H), 5.22 (s, 1H), 6.53 (s, 1H), 6.92 (s, 1H), 7.28 (s, 1H), 8.99 (s, 1H), 10.17 (s, 1H), 12.06 (s, 1H); ^{13}C NMR (DMSO- d_6) δ 173.8, 162.3, 149.9, 142.9, 135.4, 122.6, 113.3, 110.7, 105.8, 93.9, 65.2, 56.8, 28.6; HRMS m/z (ESI) calcd for $\text{C}_{15}\text{H}_{12}\text{BrN}_3\text{O}_4\text{Na}$ ($\text{M} + \text{Na}$) $^+$ 399.9909, found 399.9905.

4-(5-Bromo-2-hydroxyphenyl)-3-methyl-1,4,7,8-tetrahydro-5H-furo[3,4-b]pyrazolo[4,3-e]pyridin-5-one (13)

83% as white solid, mp = 260–262 °C. ^1H NMR (DMSO- d_6) δ : 1.82 (s, 3H), 4.78–4.98 (dd, $J=15\text{Hz}$, 2H), 5.15 (s, 1H), 6.73 (d, $J=6.3\text{ Hz}$, 1H), 6.94 (s, 1H), 9.77 (s, 1H), 7.11 (d, $J=6.3\text{ Hz}$, 1H), 9.77 (s, 1H), 10.07 (s, 1H), 11.84 (s, 1H); ^{13}C NMR (DMSO- d_6) δ 172.5, 161.1, 153.8, 147.6, 135.2, 132.2, 130.0, 118.2, 111.0, 103.4, 96.0, 65.6, 27.7, 10.5; HRMS m/z (ESI) calcd for $\text{C}_{15}\text{H}_{12}\text{BrN}_3\text{O}_3\text{Na}$ ($\text{M} + \text{Na}$) $^+$ 383.9960, found 383.9962.

4-(5-Bromo-2-hydroxyphenyl)-1,4,7,8-tetrahydro-5H-furo[3,4-b]pyrazolo[4,3-e]pyridin-5-one (14)

74% as white solid, mp = 243–244 °C. ^1H NMR (DMSO- d_6) δ : 4.84–5.08 (dd, $J=15\text{ Hz}$, 2H), 5.18 (s, 1H), 6.78 (d, $J=8.4\text{ Hz}$, 1H), 6.91 (d, $J=2.3\text{ Hz}$, 1H), 7.13 (dd, $J=2.3, 8.4\text{ Hz}$, 1H), 7.33 (s, 1H), 9.92 (s, 1H), 10.20 (s, 1H), 12.12 (s, 1H); ^{13}C NMR (DMSO- d_6) δ 172.6, 162.2, 153.9, 135.4, 130.7, 130.1, 118.2, 110.9, 105.9, 94.2, 65.8, 28.8; HRMS m/z (ESI) calcd for $\text{C}_{14}\text{H}_{10}\text{BrN}_3\text{O}_3\text{Na}$ ($\text{M} + \text{Na}$) $^+$ 369.9803, found 369.9815.

4-(2-Hydroxy-3-methoxyphenyl)-1,4,7,8-tetrahydro-5H-furo[3,4-b]pyrazolo[4,3-e] pyridin-5-one (15)

70% as white solid, mp = 276–278 °C. ^1H NMR (DMSO- d_6) δ : 3.78 (s, 3H), 4.89 (m, 2H), 4.89 (s, 1H), 5.23 (s, 1H), 6.47 (m, 1H), 6.64 (m, 1H), 6.75 (m, 1H), 7.31 (s, 1H), 8.65 (s, 1H), 10.13 (s, 1H), δ 12.05 (s, 1H); ^{13}C NMR (DMSO- d_6) δ 172.7, 161.8, 148.3, 143.4,

133.4, 120.2, 119.3, 110.3, 106.6, 95.0, 65.7, 56.5, 28.6; HRMS m/z (ESI) calcd for $C_{15}H_{13}N_3O_4Na$ ($M + Na$)⁺ 322.0804, found 322.0803.

4-(3,5-Dibromo-2-hydroxyphenyl)-1,4,7,8-tetrahydro-5H-furo[3,4-*b*]pyrazolo[4,3-*e*]pyridin-5-one (16)

76% as white solid, mp = 252–254 °C. ¹H NMR (DMSO-*d*₆) δ: 4.82–5.03 (dd, *J* = 15 Hz, 2H), 5.34 (s, 1H), 6.96 (d, *J* = 1.2 Hz, 1H), 7.34 (s, 1H), 7.50 (d, *J* = 1.2 Hz, 1H), 9.43 (s, 1H), 10.19 (s, 1H), 12.10 (s, 1H); ¹³C NMR (DMSO-*d*₆) δ: 172.8, 162.1, 150.8, 138.4, 132.6, 130.7, 113.7, 112.3, 105.1, 95.2, 66.0, 29.7; HRMS m/z (ESI) calcd for $C_{14}H_9Br_2N_3O_3Na$ ($M + Na$)⁺ 447.8908, found 447.8901.

4-(4-Bromo-2-thienyl)-1,4,7,8-tetrahydro-5H-furo[3,4-*b*]pyrazolo[4,3-*e*]pyridin-5-one (17)

10% as pink solid, mp = 264–266 °C. ¹H NMR (DMSO-*d*₆) δ: 4.81–4.93 (dd, *J* = 15 Hz, 2H), 5.30 (s, 1H), 6.98 (s, 1H), 7.43 (s, 1H), 7.55 (s, 1H), 10.4 (s, 1H), 12.37 (s, 1H). ¹³C NMR (DMSO-*d*₆) δ: 30.2, 65.4, 94.7, 104.7, 108.4, 122.2, 126.2, 128.2, 146.8, 153.0, 160.8, 172.3; HRMS m/z (ESI) calcd for $C_{12}H_8BrN_3O_2SNa$ ($M + Na$)⁺ 361.9575, found 361.9566.

General Procedure for the Other Heterocyclic Scaffold Synthesis

A mixture of a selected amino derivative (1 mmol), tetronic acid (1.1 mmol) and a corresponding aldehyde (1.1 mmol) in EtOH (4 mL) was refluxed for 12–36 h. The reaction mixture was allowed to cool to rt, and the precipitated product was collected by vacuum filtration and washed with EtOH (3 mL) and Et₂O at rt. In several cases (**34**, **35**, **37**, **38**, **39**), the products were >98% pure as judged by NMR analysis. In the other cases, they were purified by flash chromatography on silica gel with the indicated solvent system.

7-(3,4,5-Trimethoxyphenyl)-7,11-dihydrobenzo[*h*]furo[3,4-*b*]quinolin-8(10*H*)-one (18)

14% as white solid, mp = 256–258 °C, (CHCl₃/MeOH=20/1); ¹H NMR (DMSO-*d*₆) δ: 3.51 (s, 3H, OCH₃), 3.59 (s, 6H, OCH₃), 4.88–5.06 (m, 3H, CH+CH₂), 6.47 (s, 2H, CH_{Ar}), 7.13–7.52 (m, 4H, CH_{Naph}), 7.77 (d, *J* = 7.4 Hz, 1H, CH_{Naph}), 8.19 (d, 1H, *J* = 8.2 Hz, CH_{Naph}), 10.24 (s, 1H, NH); ¹³C NMR (DMSO-*d*₆) δ: 56.3 (OCH₃), 60.4 (OCH₃), 66.2 (OCH₂), 96.7 (C=C-NH), 105.8 (C_{Ar}), 119.7 (C_{Ar}), 121.6 (C_{Ar}), 123.3 (C_{Ar}), 126.6 (C_{Ar}), 128.8 (C_{Ar}), 131.4 (C_{Ar}), 133.1 (C_{Ar}), 136.7 (C_{Ar}), 143.1 (C_{Ar}), 153.3 (C_{Ar}), 159.1 (C_{Ar}), 172.6 (C=O); HRMS m/z (ESI) calc'd for $C_{24}H_{21}NO_5Na$ ($M+Na$)⁺ 426.1317, found 426.1321.

7-(3,5-Dibromophenyl)-7,11-dihydrobenzo[*h*]furo[3,4-*b*]quinolin-8(10*H*)-one (19)

39% as pink solid, mp = more 300 °C, (CHCl₃/MeOH=20/1). ¹H NMR (DMSO-*d*₆) δ: 4.88–5.09 (dd, *J* = 15 Hz, 2H), 5.31 (s, 1H), 7.17 (d, *J* = 9.0 Hz, 1H), 7.48–7.61 (m, 6H), 7.86 (d, *J* = 6 Hz, 1H), 8.24 (d, *J* = 9 Hz, 1H), 10.33 (s, 1H); ¹³C NMR (DMSO-*d*₆) δ: 69.9, 114.8, 122.3, 122.6, 123.8, 125.1, 128.0, 128.9, 130.0, 130.3, 131.5, 134.0, 134.1, 136.2, 145.2, 149.6, 163.9, 167.9; HRMS m/z (ESI) calcd for $C_{21}H_{13}Br_2NO_2Na$ ($M + Na$)⁺ 491.9211, found 491.9216.

7-(3-Bromo-4,5-dimethoxyphenyl)-7,11-dihydrobenzo[*h*]furo[3,4-*b*]quinolin-8(10*H*)-one (20)

22% as yellow solid, mp = 276–278 °C, (CHCl₃/MeOH=20/1). ¹H NMR (DMSO-*d*₆) δ: 3.69 (s, 3H), 3.76 (s, 3H), 4.91–5.17 (m, 3H), 6.84 (s, 1H), 7.06 (s, 1H), 7.20 (d, *J* = 6 Hz, 1H), 7.45–7.83 (m, 3H), 7.83 (d, *J* = 9 Hz, 1H), 8.19 (d, *J* = 9.0 Hz), 10.23 (s, 1H); ¹³C NMR (DMSO-*d*₆) δ: 56.6, 60.5, 66.3, 96.4, 112.8, 117.3, 119.2, 121.5, 123.1, 123.5, 123.8, 126.8, 128.8, 131.5, 133.2, 144.7, 144.9, 153.7, 159.3, 172.6; HRMS m/z (ESI) calcd for $C_{23}H_{18}BrNO_4Na$ ($M + Na$)⁺ 474.0317, found 474.0311.

7-(3,5-Dibromo-2-hydroxyphenyl)-7,11-dihydrobenzo[*h*]furo[3,4-*b*]quinolin-8(10*H*)-one (21)

41% as white solid, mp = 160–162 °C, (CHCl₃/MeOH=20/1); ¹H NMR (DMSO-*d*₆) δ: 4.97–5.16 (dd, *J* = 15 Hz, 2H), 5.69 (s, 1H), 7.46–7.17 (m, 2H), 7.46–7.64 (m, 4H), 7.85 (d, *J* = 9 Hz, 1H), 7.95 (s, 1H), 8.21 (d, *J* = 9 Hz, 1H), 9.73 (s, 1H), 10.34 (s, 1H); ¹³C NMR (DMSO-*d*₆) δ: 34.5, 66.5, 70.4, 95.7, 112.3, 113.8, 116.2, 119.5, 121.4, 123.6, 126.7, 128.0, 128.7, 130.6, 131.4, 132.3, 133.1, 139.1, 150.6, 160.0, 164.4, 172.6; HRMS *m/z* (ESI) calcd for C₂₁H₁₃Br₂NO₃Na (M + Na)⁺ 507.9160, found 507.9160.

7-(5-Bromo-2-hydroxy-3-methoxyphenyl)-7,11-dihydrobenzo[*h*]furo[3,4-*b*]quinolin-8(10*H*)-one (22)

74% as white solid, mp = 276–278 °C, (CHCl₃/MeOH=20/1). ¹H NMR (DMSO-*d*₆) δ: 3.73 (s, 3H), 4.87–5.08 (dd, *J* = 15 Hz, 2H), 5.54 (s, 1H), 6.64 (s, 1H), 6.84 (s, 1H), 7.15–7.52 (m, 4H), 7.72–7.78 (m, 1H), 8.12 (d, *J* = 9 Hz, 1H), 9.08 (s, 1H), 10.12 (s, 1H); ¹³C NMR (DMSO-*d*₆) δ: 33.2, 56.7, 66.3, 95.9, 110.7, 113.2, 120.4, 121.4, 123.0, 123.5, 124.1, 126.7, 128.2, 128.7, 131.1, 133.1, 136.1, 142.7, 149.2, 159.9, 172.5; HRMS *m/z* (ESI) calcd for C₂₂H₁₇BrNO₄ (M + H)⁺ 438.0341, found 438.0346.

7-(5-Bromo-2-hydroxyphenyl)-7,11-dihydrobenzo[*h*]furo[3,4-*b*]quinolin-8(10*H*)-one (23)

68% as pink solid, mp = 95–97 °C, (CHCl₃/MeOH=20/1); ¹H NMR (DMSO-*d*₆) δ: 4.86–5.07 (dd, *J* = 15 Hz, 2H), 5.46 (s, 1H), 6.71 (d, 9.0 Hz, 1H), 7.00–7.19 (m, 3H), 7.35–7.51 (m, 3H), 7.74 (d, *J* = 8.0 Hz, 1H), 8.20 (d, *J* = 9.0 Hz, 1H), 9.89 (s, 1H), 10.01 (s, 1H); ¹³C NMR (DMSO-*d*₆) δ: 33.4, 66.27, 95.91, 111.0, 118.2, 120.4, 121.4, 123.0, 123.5, 126.7, 128.2, 128.7, 130.6, 131.2, 132.5, 133.1, 136.6, 153.6, 160.4, 172.5; HRMS *m/z* (ESI) calcd for C₂₁H₁₄BrNO₃Na (M + Na)⁺ 430.0055, found 430.0050.

7-(5-Bromo-3-pyridinyl)-7,11-dihydrobenzo[*h*]furo[3,4-*b*]quinolin-8(10*H*)-one (24)

35% as white solid, mp = 262–264 °C, decomp. (CHCl₃/MeOH=20/1); ¹H NMR (DMSO-*d*₆) δ: 4.97–5.15 (dd, *J* = 15 Hz, 2H), 5.35 (s, 1H), 7.16 (d, *J* = 9 Hz, 1H), 7.49–7.65 (m, 3H), 7.84–7.87 (m, 2H), 8.28 (d, *J* = 9.0 Hz, 1H), 8.52–8.55 (m, 2H); ¹³C NMR (DMSO-*d*₆) δ: 37.9, 66.6, 95.5, 118.2, 121.1, 121.8, 123.2, 123.8, 127.0, 127.1, 128.6, 128.9, 131.9, 133.3, 138.4, 144.4, 148.3, 149.1, 159.8, 172.5; HRMS *m/z* (ESI) calcd for C₂₀H₁₃BrN₂O₂Na (M + Na)⁺ 415.0058, found 415.0054.

7-(4-Bromo-2-thienyl)-7,11-dihydrobenzo[*h*]furo[3,4-*b*]quinolin-8(10*H*)-one (25)

56% as yellow solid, mp = 268–269 °C, (CHCl₃/MeOH=20/1); ¹H NMR (DMSO-*d*₆) δ: 4.96–5.12 (dd, *J* = 15 Hz, 2H), 5.54 (s, 1H), 7.04 (s, 1H), 7.33–7.64 (m, 5H), 7.89 (d, *J* = 9 Hz, 1H), 8.21 (d, *J* = 9 Hz, 1H), 10.38 (s, 1H); ¹³C NMR (DMSO-*d*₆) δ: 35.6, 66.2, 95.9, 108.7, 118.5, 121.4, 123.0, 123.2, 123.7, 126.6, 127.0, 128.6, 128.8, 131.2, 133.3, 153.4, 159.2, 172.3; HRMS *m/z* (ESI) calcd for C₁₉H₁₂BrNO₂SK (M + K)⁺ 435.9409, found 435.9414.

2-Hydroxy-7-(3,4,5-trimethoxyphenyl)-7,11-dihydrobenzo[*h*]furo[3,4-*b*]quinolin-8(10*H*)-one (26)

63% as white solid, mp = >300 °C, (CHCl₃/MeOH=20/1); ¹H NMR (DMSO-*d*₆) δ: 3.77 (s, 6H, OCH₃), 3.67 (s, 3H, OCH₃), 4.97–5.10 (m, 3H, CH+CH₂), 6.53 (s, 2H, CH_{Ar}), 7.02 (d, *J* = 9.0 Hz, 1H, CH_{Naph}), 7.13 (d, *J* = 9.0 Hz, 1H, CH_{Naph}), 7.37 (d, *J* = 9.0 Hz, 1H, CH_{Naph}), 7.42 (s, 1H, CH_{Naph}), 7.70 (d, *J* = 9 Hz, 1H, CH_{Naph}), 9.84 (s, 1H, OH), 9.98 (s, 1H, NH); ¹³C NMR (DMSO-*d*₆) δ: 56.3 (OCH₃), 60.4 (OCH₃), 66.2 (OCH₂), 96.4 (C=C-NH), 103.9 (C_{Ar}), 105.7 (C_{Ar}), 118.8 (C_{Ar}), 119.8 (C_{Ar}), 123.2 (C_{Ar}), 124.8 (C_{Ar}), 125.4 (C_{Ar}), 127.6 (C_{Ar}), 129.9 (C_{Ar}), 130.3 (C_{Ar}), 136.6 (C_{Ar}), 143.2 (C_{Ar}), 153.3 (C_{Ar}), 156.3

(C_{Ar}), 159.2 (C_{Ar}), 172.7 (C=O); HRMS *m/z* (ESI) calcd for C₂₄H₂₁NO₆Na (M + Na)⁺ 442.1267, found 442.1267.

7-(3,5-Dibromophenyl)-2-hydroxy-7,11-dihydrobenzo[*h*]furo[3,4-*b*]quinolin-8(10*H*)-one (27)

50% as yellow solid, mp = >300 °C, (CHCl₃/MeOH=20/1); ¹H NMR (DMSO-*d*₆) δ: 4.92–5.12 (dd, *J* = 15 Hz, 2H), 5.24 (s, 1H), 6.88 (d, *J* = 9.0 Hz, 1H), 7.16 (d, *J* = 9.0 Hz, 1H), 7.37–7.71 (m, 6H), 9.90 (s, 1H), 10.09 (s, 1H); ¹³C NMR (DMSO-*d*₆) δ: 66.5, 95.5, 103.9, 118.6, 119.2, 123.2, 123.8, 125.2, 130.3, 130.5, 132.1, 151.6, 159.7, 172.6; HRMS *m/z* (ESI) calcd for C₂₁H₁₃Br₂NO₃Na (M + Na)⁺ 507.9160, found 507.9160.

7-(3-Bromo-4,5-dimethoxyphenyl)-2-hydroxy-7,11-dihydrobenzo[*h*]furo[3,4-*b*]quinolin-8(10*H*)-one (28)

34% as yellow solid, mp = >300 °C, (CHCl₃/MeOH=20/1); ¹H NMR (DMSO-*d*₆) δ: 3.67 (s, 3H), 3.80 (s, 3H), 4.94–5.12 (dd, *J* = 15 Hz, 2H), 5.16 (s, 1H), 6.85 (s, 1H), 6.99 (d, *J* = 9.0 Hz, 1H), 7.08 (s, 1H), 7.16 (d, *J* = 9.0 Hz, 1H), 7.40 (d, *J* = 9.0 Hz, 1H), 7.44 (s, 1H), 7.72 (d, *J* = 9.0 Hz, 1H), 9.88 (s, 1H), 10.05 (s, 1H); ¹³C NMR (DMSO-*d*₆) δ: 40.9, 56.5, 60.4, 66.2, 96.0, 103.8, 112.7, 117.2, 118.9, 119.2, 123.4, 124.8, 125.3, 130.0, 130.3, 144.5, 144.9, 153.6, 156.4, 159.3, 172.6; HRMS *m/z* (ESI) calcd for C₂₁H₁₃Br₂NO₄Na (M + Na)⁺ 490.0266, found 490.0268.

7-(3,5-Dibromo-2-hydroxyphenyl)-2-hydroxy-7,11-dihydrobenzo[*h*]furo[3,4-*b*]quinolin-8(10*H*)-one (29)

42% as yellow solid, mp = 278–279 °C, (CHCl₃/MeOH=20/1). ¹H NMR (DMSO-*d*₆) δ: 4.82–5.01 (dd, *J* = 15 Hz, 2H), 5.56 (s, 1H), 6.78–7.57 (m, 7H), 9.61 (s, 1H), 9.74 (s, 1H), 9.91 (s, 1H); ¹³C NMR (DMSO-*d*₆) δ: 34.6, 66.5, 95.4, 103.7, 112.2, 118.9, 119.7, 123.6, 124.6, 124.7, 127.7, 129.9, 130.3, 132.3, 132.9, 139.2, 150.5, 156.5, 160.0, 172.8; HRMS *m/z* (ESI) calcd for C₂₁H₁₃Br₂NO₄Na (M + Na)⁺ 523.9109, found 523.9100.

7-(5-Bromo-2-hydroxy-3-methoxyphenyl)-2-hydroxy-7,11-dihydrobenzo[*h*]furo[3,4-*b*]quinolin-8(10*H*)-one (30)

58% as yellow solid, mp = 215–217 °C, (CHCl₃/MeOH=20/1); ¹H NMR (DMSO-*d*₆) δ: 3.84 (s, 3H), 4.95–5.15 (dd, *J* = 15 Hz, 2H), 5.59 (s, 1H), 6.71 (d, *J* = 3.0 Hz, 1H), 6.94 (d, *J* = 3.0 Hz, 1H), 7.04 (d, *J* = 9.0 Hz, 1H), 7.15 (d, *J* = 9.0 Hz, 1H), 7.36 (d, *J* = 9.0 Hz, 1H), 7.43 (s, 1H), 7.70 (d, *J* = 9.0 Hz, 1H), 9.14 (s, 1H), 9.85 (s, 1H), 9.96 (s, 1H); ¹³C NMR (DMSO-*d*₆) δ: 56.1, 65.7, 95.0, 103.2, 110.1, 112.5, 118.2, 120.0, 122.9, 123.5, 124.2, 127.1, 129.2, 129.7, 132.0, 135.7, 142.1, 148.6, 155.8, 159.5, 172.0; HRMS *m/z* (ESI) calcd for C₂₂H₁₆BrNO₅Na (M + Na)⁺ 476.0110, found 476.0106.

7-(5-Bromo-2-hydroxyphenyl)-2-hydroxy-7,11-dihydrobenzo[*h*]furo[3,4-*b*]quinolin-8(10*H*)-one (31)

42% as orange solid, mp = 288–289 °C, decomp. (CHCl₃/MeOH=20/1); ¹H NMR (DMSO-*d*₆) δ: 4.92–5.13 (dd, *J* = 15 Hz, 2H), 5.51 (s, 1H), 6.79 (d, *J* = 6.0 Hz, 1H), 7.02–7.41 (m, 6H), 7.67 (d, *J* = 6.0 Hz, 1H), 9.80 (s, 1H), 9.93 (s, 1H); ¹³C NMR (DMSO-*d*₆) δ: 33.4, 66.4, 95.7, 103.8, 110.0, 118.2, 118.9, 120.6, 123.5, 124.8, 127.7, 129.8, 130.3, 130.5, 132.5, 136.8, 153.6, 156.4, 160.1, 172.6; HRMS *m/z* (ESI) calcd for C₂₁H₁₄BrNO₄Na (M + Na)⁺ 446.0004, found 446.0013.

7-(5-Bromo-3-pyridinyl)-2-hydroxy-7,11-dihydrobenzo[*h*]furo[3,4-*b*]quinolin-8(10*H*)-one (32)

28% as white solid, mp = >300 °C, decomp. (CHCl₃/MeOH=20/1); ¹H NMR (DMSO-*d*₆) δ: 4.92–5.12 (dd, *J* = 15 Hz, 2H), 5.248 (s, 1H), 6.88 (d, *J* = 9.0 Hz, 1H), 7.16 (d, *J* = 9.0 Hz, 1H), 7.37–7.71 (m, 6H), 9.90 (s, 1H), 10.09 (s, 1H); ¹³C NMR (DMSO-*d*₆) δ: 66.5, 95.5,

103.9, 118.6, 119.2, 123.2, 123.8, 125.2, 130.3, 130.5, 132.1, 151.6, 159.7, 172.6; HRMS m/z (ESI) calcd for $C_{23}H_{19}BrNO_5Na$ ($M + Na$)⁺ 490.0266, found 490.0268.

7-(4-Bromo-2-thienyl)-2-hydroxy-7,11-dihydrobenzo[*h*]furo[3,4-*b*]quinolin-8(10*H*)-one (33)

33% as yellow solid, mp = 273–274 °C, (CHCl₃/MeOH=20/1); ¹H NMR (DMSO-*d*₆) δ: 4.92–5.09 (dd, *J* = 15 Hz, 2H), 5.48 (s, 1H), 7.01 (s, 1H), 7.08–7.16 (m, 2H), 7.41–7.44 (d, *J* = 7.0 Hz, 3H), 7.70 (d, *J* = 9.0 Hz, 1H), 9.88 (s, 1H), 10.15 (s, 1H); ¹³C NMR (DMSO-*d*₆) δ: 35.8, 66.3, 95.6, 103.9, 108.7, 118.7, 119.2, 123.2, 123.7, 124.8, 125.2, 126.6, 129.9, 130.5, 153.6, 156.6, 159.3, 172.4; HRMS m/z (ESI) calcd for $C_{19}H_{12}BrNO_3SNa$ ($M + Na$)⁺ 435.9619, found 435.9623.

4-Hydroxy-7-(3,4,5-trimethoxyphenyl)-7,11-dihydrobenzo[*h*]furo[3,4-*b*]quinolin-8(10*H*)-one(34)

59% as brown solid, mp = >300 °C; ¹H NMR (DMSO-*d*₆) δ: 3.59 (s, 3H, OCH₃), 3.69 (s, 6H, OCH₃), 4.93–5.09 (dd, *J* = 15 Hz, 2H, CH₂), 5.48 (s, 1H, CH), 6.53 (s, 2H, CH_{Ar}), 6.88 (d, *J* = 7.1, CH_{Ar}), 7.37 (d, *J* = 8.8 Hz, 1H, CH_{Ar}), 7.38 (t, *J* = 8.3 Hz, 1H, CH_{Ar}), 7.61 (d, *J* = 8.5 Hz, 1H, CH_{Ar}), 7.71 (d, *J* = 8.5 Hz, 1H, CH_{Ar}), 10.05 (s, 1H, OH), 10.15 (s, 1H, NH); ¹³C NMR (DMSO-*d*₆) δ: 56.3 (OCH₃), 60.4 (OCH₃), 66.2 (OCH₂), 96.6 (C=C-NH), 105.8 (C_{Ar}), 109.1 (C_{Ar}), 112.0 (C_{Ar}), 117.5 (C_{Ar}), 119.9 (C_{Ar}), 124.6 (C_{Ar}), 127.2 (C_{Ar}), 127.3.3 (C_{Ar}), 131.1 (C_{Ar}), 136.7 (C_{Ar}), 143.1 (C_{Ar}), 153.3 (C_{Ar}), 154.1 (C_{Ar}), 159.1 (C_{Ar}), 172.7 (C=O); HRMS m/z (ESI) calcd for $C_{24}H_{21}NO_6Na$ ($M + Na$)⁺ 442.1267, found 442.1273.

7-(3,5-Dibromophenyl)-4-hydroxy-7,11-dihydrobenzo[*h*]furo[3,4-*b*]quinolin-8(10*H*)-one (35)

77% as brown solid, mp = >300 °C; ¹H NMR (DMSO-*d*₆) δ: 4.91–5.11 (dd, *J* = 15 Hz, 2H), 5.25 (s, 1H), 6.90 (d, *J* = 9.0 Hz, 1H), 7.04 (d, *J* = 9.0 Hz, 1H), 7.36–7.72 (m, 6H), 10.15 (s, 1H), 10.21 (s, 1H); ¹³C NMR (DMSO-*d*₆) δ: 66.5, 95.7, 109.4, 112.0, 118.0, 118.6, 123.2, 124.7, 127.1, 127.6, 130.5, 131.5, 132.1, 151.8, 154.2, 160.0, 172.6; HRMS m/z (ESI) calcd for $C_{21}H_{13}Br_2NO_3Na$ ($M + Na$)⁺ 507.9160, found 507.9152.

5-Amino-7-(3,5-dibromophenyl)-7,11-dihydrobenzo[*h*]furo[3,4-*b*]quinolin-8(10*H*)-one (37)

66% as brown solid, mp = 242–244 °C, decomp. ¹H NMR (DMSO-*d*₆) δ: 4.76–5.02 (dd, *J* = 15 Hz, 2H, CH₂), 5.34 (s, 1H, CH), 6.14 (s, 1H, CH_{Naph}), 7.27–7.30 (m, 5H, CH_{Ar}), 7.91–7.70 (m, 3H, CH_{Ar}), 9.88 (s, 1H, NH); ¹³C NMR (DMSO-*d*₆) δ: 66.1 (OCH₂), 93.6 (C=C-NH), 109.3 (C_{Ar}), 119.8 (C_{Ar}), 121.4 (C_{Ar}), 121.6 (C_{Ar}), 123.0 (C_{Ar}), 123.1 (C_{Ar}), 123.5 (C_{Ar}), 124.0 (C_{Ar}), 124.9 (C_{Ar}), 126.7 (C_{Ar}), 130.5 (C_{Ar}), 131.8 (C_{Ar}), 141.4 (C_{Ar}), 151.8 (C_{Ar}), 158.7 (C_{Ar}), 172.7 (C=O); HRMS m/z (ESI) calcd for $C_{21}H_{15}Br_2N_2O_2$ ($M + H$)⁺ 484.9500, found 484.9492.

11-(3,4,5-Trimethoxyphenyl)-8,11-dihydrobenzo[*f*]furo[3,4-*b*]quinolin-10(7*H*)-one (38)

62% as white solid, mp = 263–264 °C; ¹H NMR (DMSO-*d*₆) δ: 3.55 (s, 3H), 3.58 (s, 6H), 4.92–5.02 (dd, *J* = 15 Hz, 2H, CH₂), 5.64 (s, 1H, CH), 6.47 (s, 2H, CH_{Ar}), 7.28–7.42 (m, 3H, CH_{Naph}), 7.85–7.88 (m, 3H, CH_{Naph}), 10.28 (s, 1H, NH); ¹³C NMR (DMSO-*d*₆) δ: 36.8 (CH), 56.2 (OCH₃), 60.1 (OCH₃), 65.4 (OCH₂), 97.6 (C=C-NH), 105.7 (C_{Ar}), 115.0 (C_{Ar}), 118.1 (C_{Ar}), 123.7 (C_{Ar}), 124.3 (C_{Ar}), 127.3 (C_{Ar}), 128.6 (C_{Ar}), 129.4 (C_{Ar}), 131.1 (C_{Ar}), 132.5 (C_{Ar}), 135.2 (C_{Ar}), 136.1 (C_{Ar}), 142.0 (C_{Ar}), 153.3 (C_{Ar}), 157.6 (C_{Ar}), 172.6 (C=O); HRMS m/z (ESI) calcd for $C_{24}H_{21}NO_5Na$ ($M + Na$)⁺ 426.1317, found 426.1309.

11-(3,5-Dibromophenyl)-8,11-dihydrobenzo[*f*]furo[3,4-*b*]quinolin-10(7*H*)-one (39)

78% as pink solid, mp = 294–296 °C; ¹H NMR (DMSO-*d*₆) δ: 4.77–4.94 (dd, *J* = 15 Hz, 2H), 5.68 (s, 1H), 7.18–7.79 (m, 9H), 10.30 (s, 1H); ¹³C NMR (DMSO-*d*₆) δ: 36.9, 65.7,

96.5, 113.6, 118.1, 122.9, 123.5, 124.6, 127.6, 129.0, 130.1, 131.2, 131.8, 131.9, 135.6, 150.4, 158.1, 172.3; HRMS m/z (ESI) calcd for $C_{21}H_{14}Br_2NO_2$ ($M + H$)⁺ 469.9391, found 469.9386.

11-(3,4,5-Trimethoxyphenyl)-4,6,7,8,9,11-hexahydrobenzo[*g*]furo[3,4-*b*]quinolin-1(3*H*)-one (40)

13% as yellow solid, mp = 248–249 °C, decomp. ($CHCl_3/MeOH=20/1$); 1H NMR ($DMSO-d_6$) δ : 1.55 (m, 4H, CH_2), 2.40–2.43 (m, 4H, CH_2), 3.48 (s, 3H, OCH_3), 3.59 (s, 6H, OCH_3), 4.71–4.91 (m, 3H, $CH+CH_2$), 6.37 (s, 2H, CH_{Ar}), 6.48 (s, 1H, CH_{Naph}), 6.70 (s, 1H, CH_{Naph}), 9.74 (s, 1H, NH); ^{13}C NMR ($DMSO-d_6$) δ : 23.2 (CH_2), 28.7 (CH_2), 28.9 (CH), 56.3 (OCH_3), 60.3 (OCH_3), 65.5 (OCH_2), 95.1 ($C=C-NH$), 105.3 (C_{Ar}), 116.4 (C_{Ar}), 122.3 (C_{Ar}), 131.1 (C_{Ar}), 131.9 (C_{Ar}), 132.0 (C_{Ar}), 134.0 (C_{Ar}), 136.3 (C_{Ar}), 136.4 (C_{Ar}), 143.4 (C_{Ar}), 153.2 (C_{Ar}), 153.3 (C_{Ar}), 159.1 (C_{Ar}), 172.8 (C=O); HRMS m/z (ESI) calcd for $C_{24}H_{25}NO_5Na$ ($M + Na$)⁺ 430.1630, found 430.1626.

11-(3,5-Dibromophenyl)-4,6,7,8,9,11-hexahydrobenzo[*g*]furo[3,4-*b*]quinolin-1(3*H*)-one (41)

31% as white solid, mp = >300 °C, ($CHCl_3/MeOH=20/1$). 1H NMR ($DMSO-d_6$) δ : 1.62 (s, 4H), 2.50 (s, 4H), 4.83–5.00 (dd, $J = 15$ Hz, 2H), 4.99 (s, 1H), 6.62 (s, 1H), 6.69 (s, 1H), 7.38 (s, 2H), 7.61 (s, 1H), 10.05 (s, 1H); ^{13}C NMR ($DMSO-d_6$) δ : 23.1, 23.2, 28.7, 29.0, 65.8, 94.3, 116.8, 121.1, 123.1, 130.3, 131.3, 131.9, 132.5, 134.1, 137.1, 151.9, 159.5, 172.5, HRMS m/z (ESI) calcd for $C_{21}H_{13}Br_2NO_3Na$ ($M + Na$)⁺ 495.9524, found 495.9519.

6-(3,4,5-Trimethoxyphenyl)-3,6,9,10-tetrahydro-7*H*-furo[3,4-*b*]pyrrolo[2,3-*h*]quinolin-7-one (42)

56% as brown solid, mp = >300 °C, ($CHCl_3/MeOH=20/1$); δ : 3.60 (s, 3H, OCH_3), 3.69 (s, 6H, OCH_3), 4.93–5.09 (dd, $J = 15$ Hz, 2H, CH_2), 5.05 (s, 1H, CH), 6.52 (s, 2H, CH_{Ar}), 6.66 (s, 1H, $H_{\alpha-Ind}$), 6.84 (d, $J = 6.0$ Hz, 1H, CH_{Ind-7}), 7.00 (d, $J = 6.0$ Hz, 1H, CH_{Ind-6}), 7.31 (t, $J = 3.0$ Hz, 1H, $H_{\beta-Ind}$), 9.99 (s, 1H, NH), 11.15 (s, 1H, NH); ^{13}C NMR ($DMSO-d_6$) δ : 55.8 (OCH_3), 59.8 (OCH_3), 65.2 (OCH_2), 95.6 (C_{Ar}), 98.2 (C_{Ar}), 105.1 (C_{Ar}), 107.0 (C_{Ar}), 112.7 (C_{Ar}), 116.9 (C_{Ar}), 123.7 (C_{Ar}), 124.7 (C_{Ar}), 127.6 (C_{Ar}), 135.8 (C_{Ar}), 143.5 (C_{Ar}), 152.6 (C_{Ar}), 158.4 (C_{Ar}), 172.4 (C=O); HRMS m/z (ESI) calcd for $C_{22}H_{20}N_2O_5K$ ($M + K$)⁺ 431.1009, found 431.1005.

6-(3,5-Dibromophenyl)-3,6,9,10-tetrahydro-7*H*-furo[3,4-*b*]pyrrolo[2,3-*h*]quinolin-7-one (43)

39% as brown solid, mp = >300 °C, ($CHCl_3/MeOH=20/1$); δ : 4.96–5.17 (m, 3H), 6.67 (s, 2H), 7.01 (s, 1H), 7.32–7.59 (m, 4H), 10.09 (s, 1H), 11.25 (s, 1H); ^{13}C NMR ($DMSO-d_6$) δ : 66.0, 95.4, 98.8, 108.1, 112.0, 117.7, 123.0, 124.2, 125.7, 128.4, 130.4, 131.7, 136.2, 152.6, 159.4, 172.8; HRMS m/z (ESI) calcd for $C_{19}H_{12}Br_2N_2O_2Na$ ($M + Na$)⁺ 480.9163, found 480.9164.

4-(3,4,5-trimethoxyphenyl)-4,8-dihydro-1*H*-furo[3,4-*b*]pyrazolo[4,3-*e*]pyridine-3,5(2*H*,7*H*)-dione (44)

45% as pink solid, mp = 186–188 °C, ($CHCl_3/MeOH=20/1$); δ : 3.69 (s, 3H, OCH_3), 3.71 (s, 6H, OCH_3), 4.33–4.57 (m, 3H, $CH+CH_2$), 6.61 (s, 1H, CH_{Ar}), 6.77 (s, 1H, CH_{Ar}); ^{13}C NMR ($DMSO-d_6$) δ : 33.4 (CH), 56.3 (OCH_3), 60.5 (OCH_3), 68.3 (OCH_3), 89.2 (C_{Ar}), 104.8 (C_{Ar}), 105.3 (C_{Ar}), 136.3 (C_{Ar}), 142.2 (C_{Ar}), 152.9 (C_{Ar}), 155.9 (C_{Ar}), 177.5 (C=O), 181.5 (C=O); HRMS m/z (ESI) calcd for $C_{17}H_{16}N_3O_6$ ($M + H$)⁺ 358.1039, found 358.1030.

4-(3,5-Dibromophenyl)-4,8-dihydro-1H-furo[3,4-b]pyrazolo[4,3-e]pyridine-3,5(2H,7H)-dione (45)

38% as orange solid, mp = 228–230 °C, (CHCl₃/MeOH=20/1); δ : 4.31–4.46 (dd, J = 15 Hz, 2H), 5.35 (s, 3H), 7.35 (s, 1H), 7.81 (s, 2H), 7.97 (s, 1H); ¹³C NMR (DMSO-*d*₆) δ : 68.4, 69.2, 97.2, 104.1, 108.7, 121.7, 122.7, 129.1, 132.6, 134.5, 135.0, 155.0, 155.9, 168.6, 177.1, 181.9; HRMS m/z (ESI) calcd for C₁₄H₁₀Br₂N₃O₃ (M + H)⁺ 425.9089, found 425.9089.

4-Amino-2-(methylsulfanyl)-5-(3,4,5-trimethoxyphenyl)-5,9-dihydrofuro[3',4':5,6]pyrido[2,3-d]pyrimidin-6(8H)-one (46)

60% as white solid, mp = 261–262 °C, decomp. (CHCl₃/MeOH=20/1); δ : 2.35 (s, 3H, SCH₃), 3.59 (s, 3H, OCH₃), 3.69 (s, 6H, OCH₃), 3.99–4.27 (m, 3H, CH+CH₂), 5.96 (s, 1H, NH), 6.11 (s, 1H, NH), 6.66 (s, 2H, CH_{Ar}), 7.55 (s, 1H, NH); ¹³C NMR (DMSO-*d*₆) δ : 13.5 (SCH₃), 35.5 (CH), 50.7(OCH₂), 56.4 (OCH₃), 60.4 (OCH₃), 74.7 (C_{Ar}), 83.0 (C_{Ar}), 86.5 (C_{Ar}), 106.6 (C_{Ar}), 136.6 (C_{Ar}), 137.5 (C_{Ar}), 152.9 (C_{Ar}), 157.7 (C_{Ar}), 161. (C_{Ar})₁, 167.9 (C_{Ar}), 175.2 (C=O); HRMS m/z (ESI) calcd for C₁₉H₂₀N₄O₅SNa (M + Na)⁺ 439.1052, found 439.1062.

4-Amino-5-(3,5-dibromophenyl)-2-(methylsulfanyl)-5,9-dihydrofuro[3',4':5,6]pyrido [2,3-d]pyrimidin-6(8H)-one (47)

36% as white solid, mp = 205–207 °C, (CHCl₃/MeOH=20/1); δ : 2.34 (s, 3H), 4.77–4.92 (dd, J = 8.0 Hz, 2H), 5.39 (s, 1H), 7.44 (m, 2H), 7.66–7.77 (m, 2H), 8.07 (s, 1H), 10.41 (s, 1H); ¹³C NMR (DMSO-*d*₆) δ : 13.7, 33.9, 66.0, 69.7, 90.8, 99.0, 123.4, 131.0, 135.4, 148.6, 154.8, 162.6, 168.0, 175.5; HRMS m/z (ESI) calcd for C₁₆H₁₃Br₂N₄O₂S (M + H)⁺ 482.9126, found 482.9128.

Cell Culture

Human T-cell leukemia cell line Jurkat (ATCC TIB-152, E6-1 clone) was cultured in RPMI-1640 (Invitrogen) supplemented with 10% FBS (Invitrogen), 100 mg/L penicillin G, 100 mg/L streptomycin, 1.0 mM sodium pyruvate, 1.5 g/L sodium bicarbonate, and 4.5 g/L glucose (all from Sigma). Human cervical cancer cell line HeLa (ATCC S3) was cultured in DMEM (Invitrogen) supplemented with 10% FBS, 100 mg/L penicillin G, and 100 mg/L streptomycin. MCF-7 (human mammary carcinoma) cells were cultured in DMEM supplemented with 1.0 mM sodium pyruvate, 1% GlutaMaxTM-1 (Invitrogen), 100 μ g/mL penicillin, 100 μ g/mL streptomycin, and 10% FBS. The cells were incubated at 37 °C in a humidified atmosphere with 5% CO₂.

MTT Assay

100 μ L of HeLa or MCF-7 cells were transferred to each well of a 96-well microtiter plate at a concentration of 2×10^4 cells/mL and incubated for 24 h to allow proper adhesion. Cells were treated with the panel of test compounds at a series of concentrations and DMSO as control. After 48h incubation, 20 μ L of MTT reagent (5 mg/mL) was added to each well of the plates. The plate was incubated for 2 h at 37 °C. The media were removed from each well of the plate and the resulting formazan crystals were dissolved in 100 μ L of DMSO. Optical density (OD) at 490 nm was measured using a ThermoMAX microplate reader. The experiments were performed in eight replicates and repeated at least twice for each compound per cell line.

Annexin-V Apoptosis Assay

2×10^5 Jurkat cells/mL were plated in 24 well plates, treated with the test compounds at a range of concentrations and incubated for 48 hours. The cells were centrifuged at 400 G for

1 min. The supernatant was discarded and the cells were resuspended in 100 μ L per sample of Annexin-V-FITC/ propidium iodide solution in HHB (3 μ L CaCl₂ (1.5 M) per mL HHB, 2 μ L (10 mg/mL) propidium iodide (Sigma) per mL HHB and 20 μ L Annexin-V-FITC (Southern Biotech) per mL HHB). The samples in the labeling solution were transferred into Falcon tubes and incubated in a water bath at 37 °C for 20 min. The samples were then analyzed using a Becton Dickinson FACscan flow cytometer with CellQuest software. The results were tabulated as % of Annexin-V-FITC positive apoptotic cells. The experiments were performed in three replicates and repeated at least twice for each compound.

Caspase-3 Activity Assay

Caspase-3 activation was detected by using a Caspase-3 colorimetric activity assay kit (Chemicon), which assays the activity of caspase-3, recognizing the sequence DEVD. The assay is based on spectrophotometric detection of *p*-nitroaniline (pNA) after cleavage of the labeled substrate DVED-p-NA. Therefore, Jurkat cells were treated with a panel of test compounds (0.1, 0.5 and 1 μ M), DMSO, and podophyllotoxin (0.1, 0.5 and 1 μ M). 1×10^6 cells were harvested and lysed with lysis buffer. Protein concentration of each sample was determined using Pierce BCA protein assay kit (Pierce). Each sample was mixed with caspase-3 substrate (DEVD-p-nitroaniline) and incubated at 37 °C for 2 h in 96 well plates (LPS). Samples were read at 405 nm using a spectrophotometer (Molecular Devices). The experiments were performed in quadruplicates and repeated at least twice for each compound.

In Vitro Tubulin Polymerization Assay

The *in vitro* tubulin polymerization assay was conducted as described by the manufacturer (Cytoskeleton Inc.). In brief, taxol, DMSO, 10, 16 and podophyllotoxin were incubated with purified bovine tubulin and buffer containing 10% glycerol and 1 mM GTP at 37 °C each in a separate experiment. The effect of each agent on tubulin polymerization was monitored in a temperature-controlled Carey Eclipse Fluorescence Spectrophotometer (Varian) for twenty minutes, with readings acquired every 15 seconds.

Morphological Analysis of Microtubule Organization in HeLa Cells

HeLa cells were cultured in DMEM supplemented with 10% fetal calf serum, sodium pyruvate, sodium bicarbonate and PSF. For dihydropyridopyrazole treatments, cells were treated for 3 hours with either carrier (0.1% DMSO) or compounds solubilized in DMSO and prediluted in media prior to fixation by immersion in methanol at -20°C. Cells were subsequently rehydrated in phosphate-buffered saline (PBS), and blocked by incubation in PBS containing 5% Bovine Serum Albumin, for one hour at 20°C. Cells were then incubated with Hoechst 33342 (Molecular Probes), mouse anti-tubulin (Sigma) and rabbit anti-Hec1 (Abcam) in PBS-BSA overnight at 4°C. Primary antibodies were detected using Alexafluor-conjugated secondary antibodies (Molecular Probes), and images were acquired using a Zeiss Axiovert 200M inverted microscope equipped with epifluorescence optics and an Apotome structured illumination module (Carl Zeiss). All acquired images were exported into eight bit tiff files and figures were prepared using Adobe Photoshop software.

Supplementary Material

Refer to Web version on PubMed Central for supplementary material.

Acknowledgments

This work is supported by the US National Institutes of Health (RR-16480 and CA-135579) under the BRIN/INBRE and AREA programs. W.A.L.v.O. gratefully acknowledges funding from the Research Office, University

of the Witwatersrand, for supporting this collaboration (postdoctoral fellowship to U.D.B.), the National Research Foundation (NRF, Pretoria) for research funding, and the Alexander van Humboldt Foundation for a Georg-Forster Experienced Researcher fellowship with Profs Herbert Waldmann and Daniel Rauh at the MPI and Technical University Dortmund. We thank Mr H. Dücker and Ms N. Martinez (MPI-Dortmund) for assistance with the chiral-prep HPLC.

Abbreviations

ATCC	American Type Culture Collection
DMEM	Dulbecco's modified Eagle's medium
DFT	density functional theory
DMF	dimethylformamide
DMSO	dimethyl sulfoxide
ECACC	European Collection of Cell Culture
EDTA	diaminoethanetetraacetic acid
EtOH	ethanol
FBS	fetal bovine serum
FITC	fluorescein isothiocyanate
HEPES	4-(2-hydroxyethyl)-1-piperazinethanesulfonic acid
HHB	Heinz-HEPES buffer
HRMS	high resolution mass spectrometry
MCR	multicomponent reaction
MTT	3-(4,5-dimethylthiazol-2-yl)-2,5-diphenyltetrazolium bromide
PDB	protein data bank
RU	relative units
SAR	structure-activity relationship
TLC	thin layer chromatography
SD	standard deviation

References

1. Koehn FE, Carter GT. The evolving role of natural products in drug discovery. *Nat Rev Drug Discovery*. 2005; 4:206–220.
2. Newman DJ, Cragg GM, Snader KM. Natural products as sources of new drugs over the period 1981–2002. *J Nat Prod*. 2003; 66:1022–1037. [PubMed: 12880330]
3. Breinbauer R, Vetter IR, Waldmann H. From protein domains to drug candidates - natural products as guiding principles in the design and synthesis of compound libraries. *Angew Chem Int Ed*. 2002; 41:2879–2890.
4. Harvey AL. Natural products in drug discovery. *Drug Discovery Today*. 2008; 13:894–901. [PubMed: 18691670]
5. (a) Magedov IV, Manpadi M, Rozhkova E, Przheval'skii NM, Rogelj S, Shors ST, Steelant WFA, Van slambrouck S, Kornienko A. Structural simplification of bioactive natural products with multicomponent synthesis: Dihydropyridopyrazole analogues of podophyllotoxin. *Bioorg Med Chem Lett*. 2007; 17:1381–1385. [PubMed: 17188868] (b) Magedov IV, Manpadi M, Van slambrouck S, Steelant WFA, Rozhkova E, Przheval'skii NM, Rogelj S, Kornienko A. Discovery and investigation of antiproliferative and apoptosis-inducing properties of new heterocyclic

- podophyllotoxin analogues accessible by a one-step multicomponent synthesis. *J Med Chem.* 2007; 50:5183–5192. [PubMed: 17894480] (c) Magedov IV, Manpadi M, Evdokimov NM, Elias EM, Rozhkova E, Ogasawara MA, Bettale JD, Przeval'skii NM, Rogelj S, Kornienko A. Antiproliferative and apoptosis inducing properties of pyrano[3,2-c]pyridones accessible by a one-step multicomponent synthesis. *Bioorg Med Chem Lett.* 2007; 17:3872–3876. [PubMed: 17512729] (d) Magedov IV, Manpadi M, Ogasawara MA, Dhawan AS, Rogelj S, Van slambrouck S, Steelant WFA, Evdokimov NM, Uglinskii PY, Elias EM, Knee EJ, Tongwa P, Antipin MY, Kornienko A. Structural simplification of bioactive natural products with multicomponent synthesis. 2. Antiproliferative and antitubulin activities of pyrano[3,2-c]pyridones and pyrano[3,2-c]quinolones. *J Med Chem.* 2008; 51:2561–2570. [PubMed: 18361483] (e) Evdokimov NM, Van slambrouck S, Heffeter P, Tu L, Le Calve B, Lamoral-Theys D, Hooten CJ, Uglinskii PY, Rogelj S, Kiss R, Steelant WFA, Berger W, Bologa CJ, Yang JJ, Kornienko A, Magedov IV. Structural simplification of bioactive natural products with multicomponent synthesis. 3. Fused uracil-containing heterocycles as novel topoisomerase-targeting agents. *J Med Chem.* 2011; 54:2012–2021. [PubMed: 21388138]
6. Bohlin L, Rosen B. Podophyllotoxin derivatives: Drug discovery and development. *Drug Discov Today.* 1996; 1:343–351.
 7. For reviews, see: (a) You YJ. Podophyllotoxin derivatives: Current synthetic approaches for new anticancer agents. *Curr Pharm Des.* 2005; 11:1695–1717. [PubMed: 15892669] (b) Gordaliza M, Castro MA, Corral JMM, San Feliciano A. Antitumor properties of podophyllotoxin and related compounds. *Curr Pharm Des.* 2000; 6:1811–1839. [PubMed: 11102564]
 8. Berkowitz DB, Maeng J-H, Dantzig AH, Shepard RL, Norman BH. Chemoenzymatic and ring E-modular approach to the (-)-podophyllotoxin skeleton. Synthesis of 3',4',5'-tridemethoxy-(-)-podophyllotoxin. *J Am Chem Soc.* 1996; 118:9426–9427.
 9. See for example: Vial JP, Belloc F, Dumain P, Besnard S, Lacombe F, Boisseau MR, Reiffers J, Bernard P. Study of the apoptosis induced in vitro by antitumoral drugs on leukaemic cells. *Leukemia Res.* 1997; 21:163–172. [PubMed: 9112434]
 10. See for example: Kemnitzer W, Drewe J, Jiang S, Zhang H, Wang Y, Zhao J, Jia S, Herich J, Labreque D, Storer R, Meerovitch K, Bouffard D, Rej R, Denis R, Blais C, Lamothe S, Attardo G, Gourdeau H, Tseng B, Kasibhatla S, Cai SX. Discovery of 4-aryl-4H-chromenes as a new series of apoptosis inducers using a cell- and caspase-based high-throughput screening assay. 1. Structure-activity relationships of the 4-aryl group. *J Med Chem.* 2004; 47:6299–6310. [PubMed: 15566300]
 11. (a) Vermes I, Haanen C, Steffens-Nakken H, Reutelingsperger C. A novel assay for apoptosis - flow cytometric detection of phosphatidylserine expression on early apoptotic cells using fluorescein-labeled annexin-V. *Immunol Methods.* 1995; 184:39–51. (b) Fadok VA, Voelker DR, Campbell PA, Cohen JJ, Bratton DL, Henson PM. Exposure of phosphatidylserine on the surface of apoptotic lymphocytes triggers specific recognition and removal by macrophages. *J Immunol.* 1992; 148:2207–2216. [PubMed: 1545126]
 12. Kasibhatla S, Gourdeau H, Meerovitch K, Drewe J, Reddy S, Qiu L, Zhang H, Bergeron F, Bouffard D, Yang Q, Herich J, Lamothe S, Cai SX, Tseng B. Discovery and mechanism of action of a novel series of apoptosis inducers with potential vascular targeting activity. *Mol Cancer Ther.* 2004; 3:1365–1373. [PubMed: 15542775]
 13. Hamel E. Evaluation of antimetabolic agents by quantitative comparisons of their effects on the polymerization of purified tubulin. *Cell Biochem Biophys.* 2003; 38:1–21. [PubMed: 12663938]
 14. (a) Frackenhof J, Adelt I, Antonicek H, Arnold C, Behrmann P, Blaha N, Bohmer J, Gutbrod O, Hanke R, Hohmann S, van Houtdrevre M, Losel P, Malsam O, Melchers M, Neufert V, Peschel E, Reckmann U, Schenke T, Thiesen HP, Velten R, Vogelsang K, Weiss HC. Insecticidal heterologous-Tubuline polymerization inhibitors with activity against chewing pests. *Bioorg Med Chem.* 2009; 17:4160–4184. [PubMed: 19223182] For the first study of the utilization of anilines in this MCR, see: (b) Tratat C, Giorgi-Renault S, Husson HP. A multicomponent reaction for the one-pot synthesis of 4-aza-2,3-didehydropodophyllotoxin and derivatives. *Org Lett.* 2002; 4:3187–3189. [PubMed: 12227745]
 15. (a) Tu S, Zhang Y, Zhang J, Jiang B, Jia R, Zhang J, Ji S. A simple procedure for the synthesis of 4-aza-podophyllotoxin derivatives in water under microwave irradiation conditions. *Synlett.* 2006:2785–2790. (b) Kozlov NG, Bondarev SL, Kadetskii AP, Basalaeva LI, Pashkovskii FS. Tetronic acid in reaction with aromatic aldehydes and 2-naphthylamine. Investigation of

- fluorescent and nonlinear-optical characteristics of compounds obtained. *Russian J Org Chem.* 2008; 44:1031–1037.
16. (a) Khurana JM, Magoo D. pTSA-catalyzed one-pot synthesis of 12-aryl-8,9,10,12-tetrahydrobenzo[a] xanthen-11-ones in ionic liquid and neat conditions. *Tetrahedron Lett.* 2009; 50:4777–4780. (b) Wang RZ, Zhang LF, Cui ZS. Iodine-catalyzed synthesis of 12-aryl-8,9,10,12-tetrahydro-benzo[a]xanthen-11-one derivatives via multicomponent reaction. *Synth Commun.* 2009; 39:2101–2107. (c) Gao S, Tsai CH, Yao CF. A simple and green approach for the synthesis of tetrahydrobenzo[a]xanthen-11-one Derivatives using tetrabutyl ammonium fluoride in water. *Synlett.* 2009:949–954. (d) Nandi GC, Samai S, Kumar R, Singh MS. An efficient one-pot synthesis of tetrahydrobenzo[a]xanthene-11-one and diazabenzo[a]anthracene-9,11-dione derivatives under solvent free condition. *Tetrahedron.* 2009; 65:7129–7134. (e) Li J, Tang W, Lu L, Su W. Strontium triflate catalyzed one-pot condensation of beta-naphthol, aldehydes and cyclic 1,3-dicarbonyl compounds. *Tetrahedron Lett.* 2008; 49:7117–7120. (f) Das B, Laxminarayana K, Krishnaiah M, Srinivas Y. An efficient and convenient protocol for the synthesis of novel 12-aryl- or 12-alkyl-8,9,10,12-tetrahydrobenzo[a]xanthen-11-one derivatives. *Synlett.* 2007:3107–3112.
17. These results will be published elsewhere.
18. Brewer CF, Loike JD, Horwitz SB. Conformational-analysis of podophyllotoxin and its congeners - structure-activity relationships in microtubule assembly. *J Med Chem.* 1979; 22:215–221. [PubMed: 423203]
19. Ravelli RBG, Gigant B, Curmi PA, Jourdain I, Lachkar S, Sobel A, Knossow M. Insight into tubulin regulation from a complex with colchicine and a stathmin-like domain. *Nature.* 2004; 428:198–202. [PubMed: 15014504]
20. (a) Alam A, Naik PK. Molecular modelling evaluation of the cytotoxic activity of podophyllotoxin analogues. *J Comput-Aided Mol Des.* 2009; 23:209–225. [PubMed: 19052697] (b) Verma RP, Hansch C. A QSAR study on the cytotoxicity of podophyllotoxin analogues against various cancer cell lines. *Med Chem.* 2010; 6:79–86. [PubMed: 20470250] (c) Villanueva HE, Setzer WN. Cembrene Diterpenoids: Conformational Studies and Molecular Docking to Tubulin. *Rec Nat Prod.* 2010; 4:115–123.
21. Kim do Y, Kim KH, Kim ND, Lee KY, Han CK, Yoon JH, Moon SK, Lee SS, Seong BL. Design and biological evaluation of novel tubulin inhibitors as antimetotic agents using pharmacophore binding model with tubulin. *J Med Chem.* 2006; 49:5664–5670. [PubMed: 16970393]

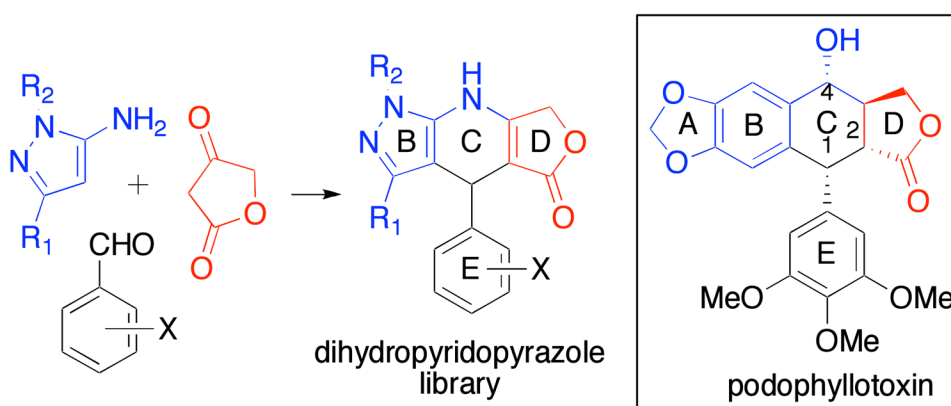


Figure 1.
Podophyllotoxin-mimetic dihydropyridopyrazole library.

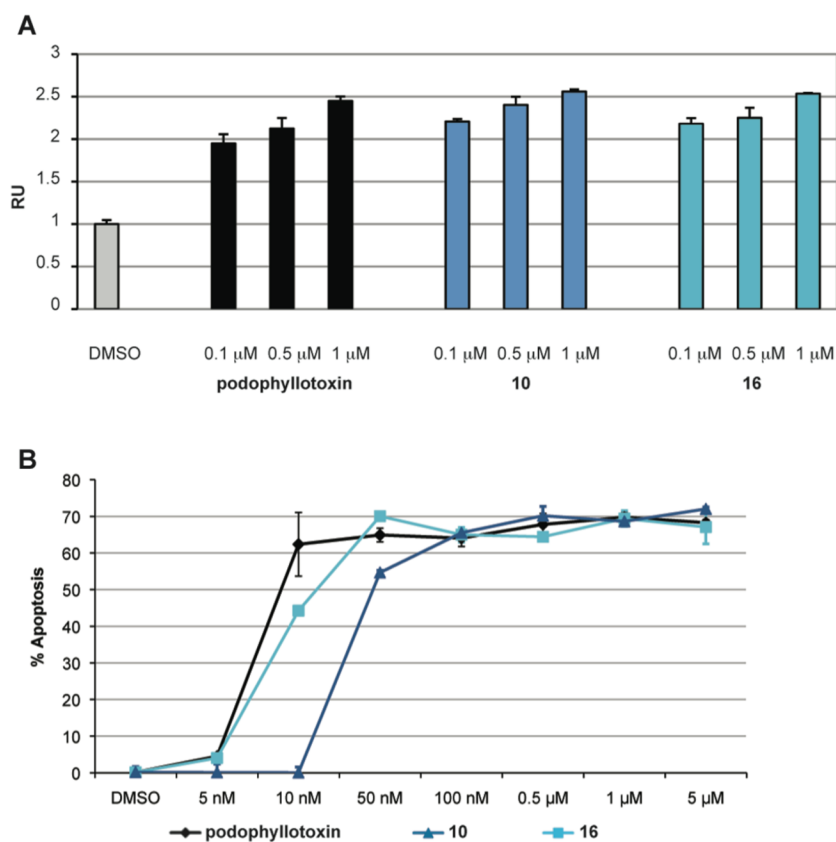


Figure 2.

(A) Caspase-3 activation in Jurkat cells with indicated compounds. The magnitudes of activation are expressed as relative units (RU) with DMSO control assigned the value of one. Error bars represent data from two independent experiments, each performed in quadruplicates. (B) % Apoptotic cells after 48 h of treatment with indicated compounds \pm SD from two independent experiments, each performed in 3 replicates, determined by flow cytometric Annexin-V/propidium iodide assay.

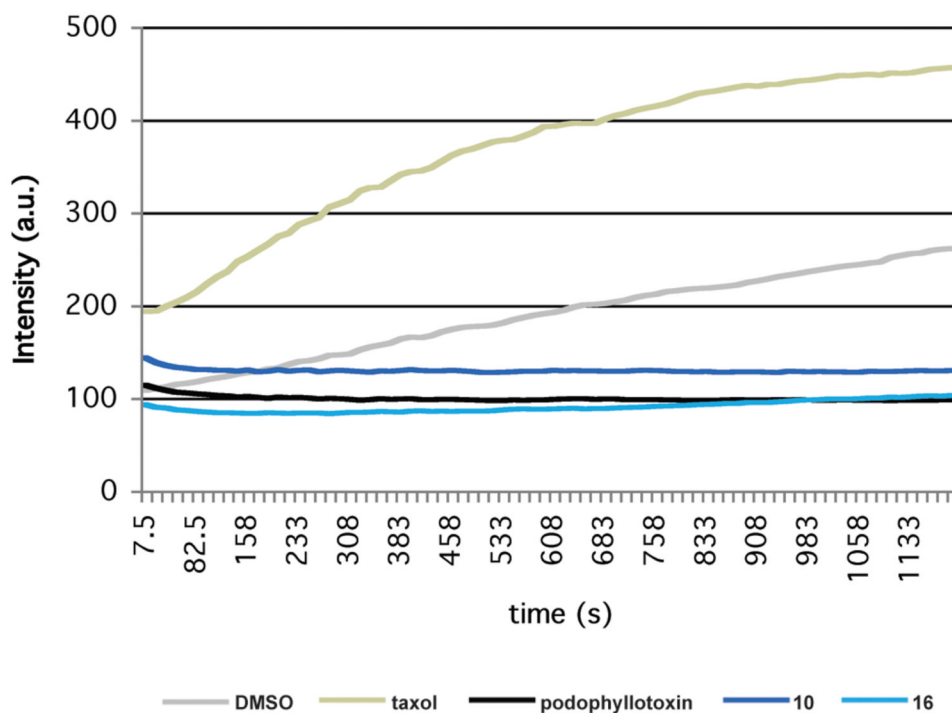


Figure 3.

Effect of dihydropyridopyrazoles on tubulin polymerization *in vitro*. Taxol (3 μ M) promotes microtubule formation relative to 0.05% DMSO control. In contrast, **10** (25 μ M), **16** (25 μ M) and podophyllotoxin (25 μ M) completely suppress tubulin polymerization.

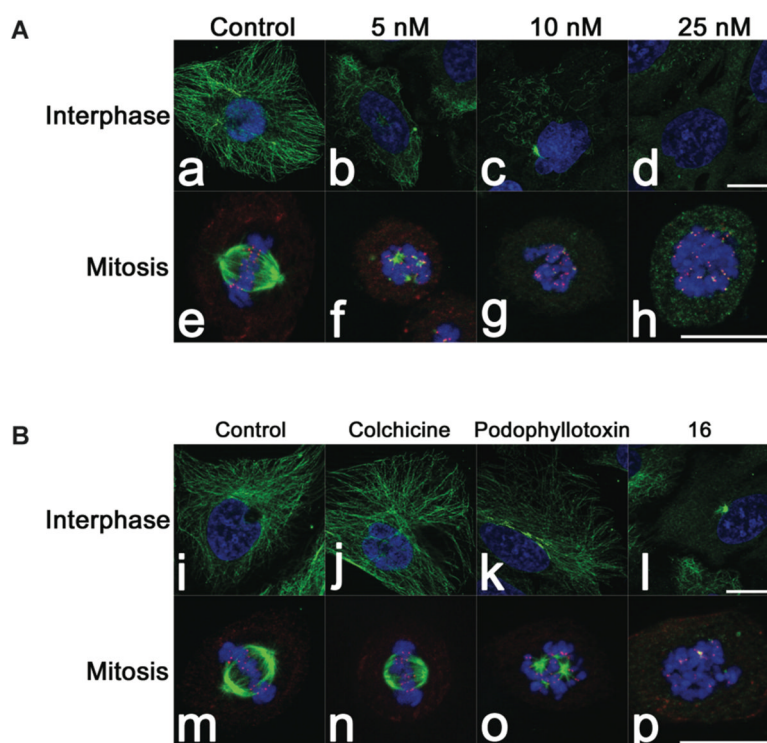


Figure 4. Microtubule organization in interphase and mitotic HeLa cells treated with (A) **16** at the indicated concentrations and (B) indicated agents at 5 nM: microtubules (green), the kinetochore marker Hec1 (red, panels e-h and m-p) and Hoechst 33342 (blue). Scale bars, 10 μm.

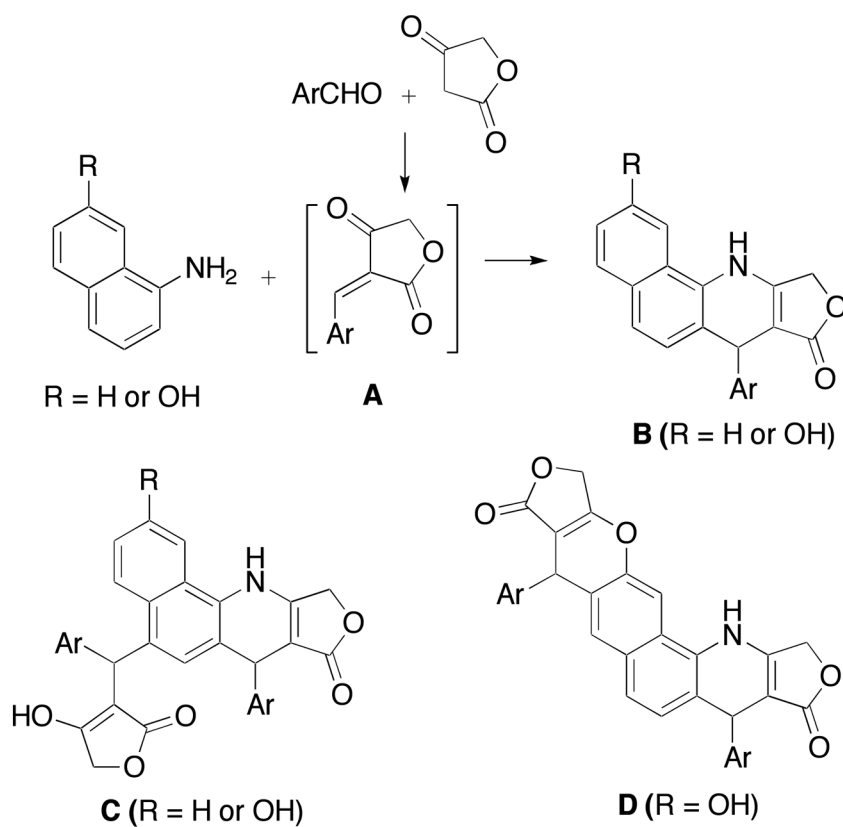


Figure 5.
MCR utilizing α -naphthylamines and possible side products.

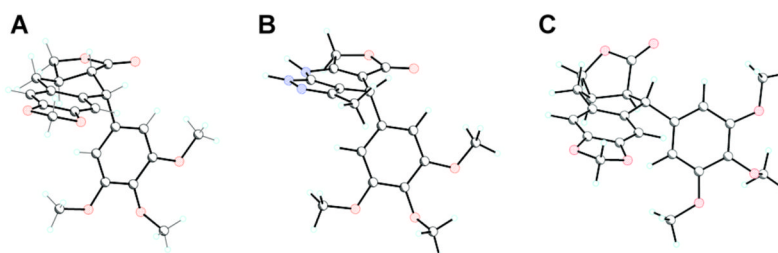


Figure 6.
DFT optimizations of molecular geometries of (A) 4-deoxypodophyllotoxin, (B) dihydropyridopyrazole **1**, and (C) 4-deoxypicropodophyllin.

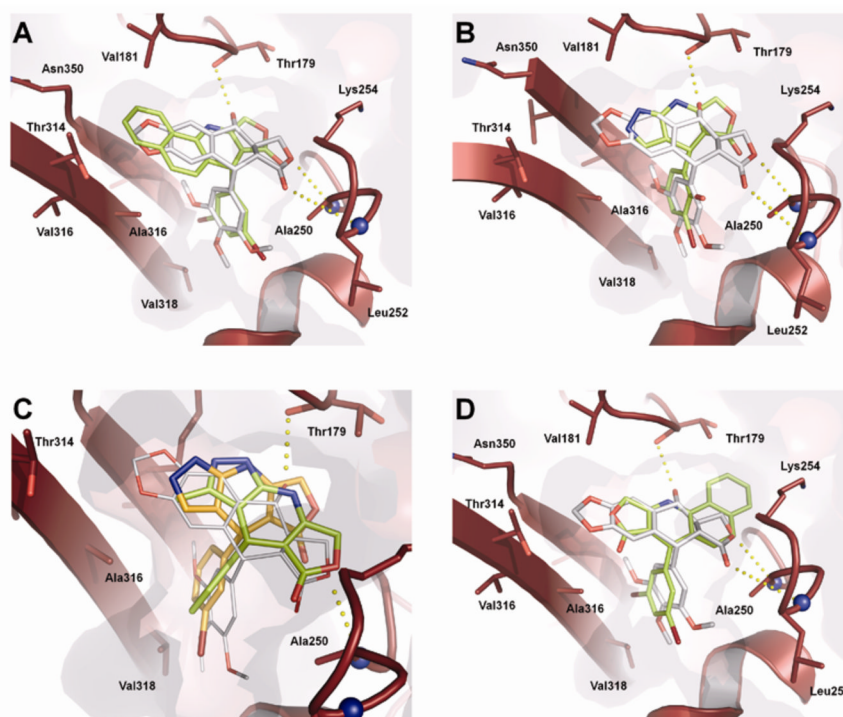


Figure 7.

Representations of molecular dockings performed in this study – all molecules overlaid with podophyllotoxin (in white): (a) *R*-**19** - representative of the binding mode of the most potent inhibitors with four ring-annulated systems; (b) *R*-**16** - representative of smaller, highly potent compounds with three ring annulated systems, binding analogous to *R*-**19**; (c) *R*-**5** (green) and *R*-**6** (orange). Compared to *R*-**6**, *R*-**5** has an additional methyl at the B ring that is responsible for a drop in potency and a twist away from the optimal binding mode [as in (a) and (b)] according to the docking study; (d) *S*-**19** – the less potent *S*-enantiomer of *R*-**19** binds in a “flipped” confirmation, relative to *R*-**19**.

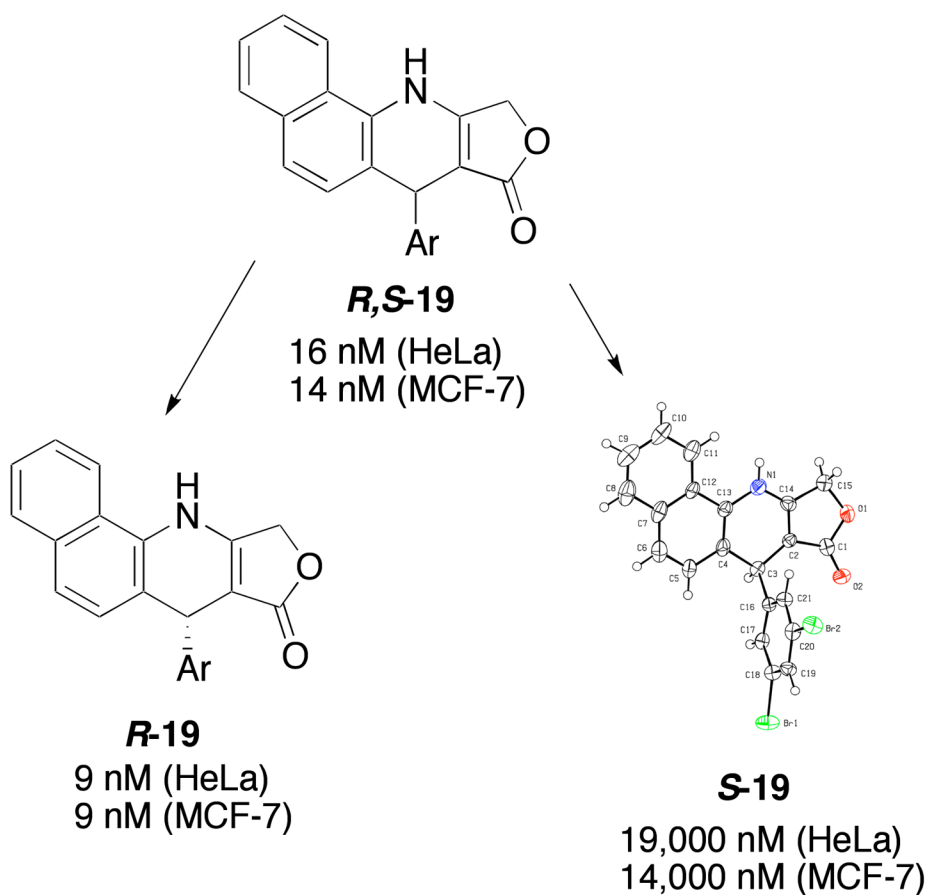
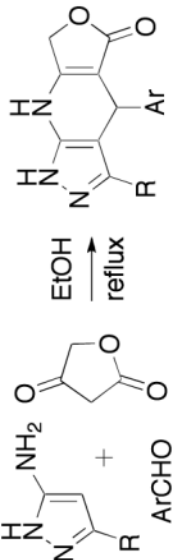
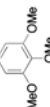
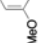
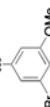
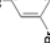
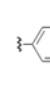

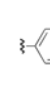

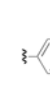

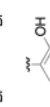

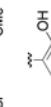

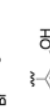
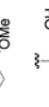
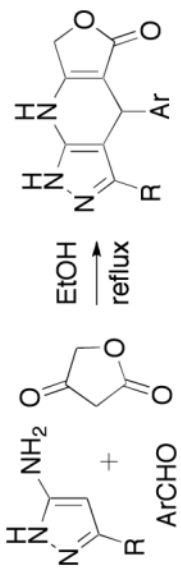
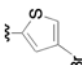


Figure 8. GI₅₀ values of *R,S*-19, *R*-19 and *S*-19 toward HeLa and MCF-7 cell lines and X-ray structure of *S*-19 (note that only one of two molecules in the unit cell is shown and that ORTEP diagram is shown at the 50% probability level).

Table 1

Synthesis and antiproliferative activity of dihydropyridopyrazoles

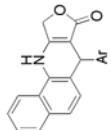
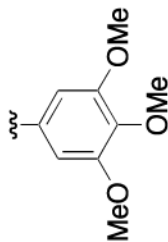
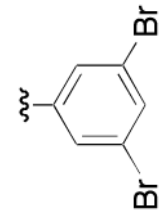
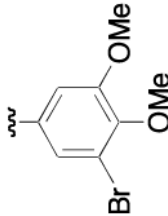
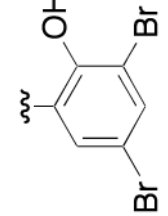
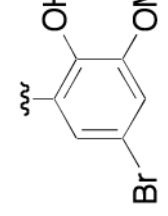
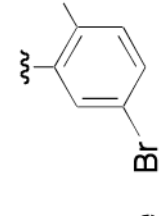
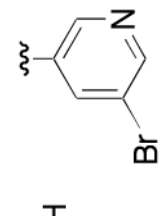
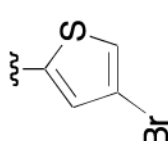
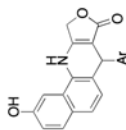
				GI_{50} (μM) ^[d]		
#	Ar	R	%	HeLa	MCF-7	
1		Me	80	5.0 \pm 0.5	5.0 \pm 0.5	
2		H	75	3.0 \pm 0.1	0.25 \pm 0.06	
3		Me	78	0.75 \pm 0.10	1.0 \pm 0.1	
4		H	72	0.75 \pm 0.05	0.25 \pm 0.06	
5		Me	76	3.0 \pm 0.1	4.0 \pm 0.3	
6		H	71	0.075 \pm 0.005	0.10 \pm 0.01	
7		Me	88	3.0 \pm 0.5	0.8 \pm 0.1	
8		H	76	0.075 \pm 0.015	0.015 \pm 0.010	
9		Me	85	0.075 \pm 0.010	0.075 \pm 0.006	
10		H	83	0.025 \pm 0.008	0.025 \pm 0.003	
11		Me	85	0.035 \pm 0.004	0.10 \pm 0.04	
12		H	81	0.025 \pm 0.003	0.030 \pm 0.005	
13		Me	83	0.30 \pm 0.08	0.25 \pm 0.05	
14		H	74	0.050 \pm 0.005	0.025 \pm 0.004	
15		H	70	2.0 \pm 0.3	0.50 \pm 0.07	
16		H	76	0.020 \pm 0.005	0.010 \pm 0.003	

				
GI ₅₀ (μM) ^[a]				
#	Ar	R	%	HeLa
17		H	10	1.15 ± 0.05
Podophyllotoxin				0.020 ± 0.002
				0.010 ± 0.003

^a Concentration required to reduce the viability of cells by 50%, after 48 h of treatment with indicated compounds, relative to DMSO control; ± SD from two independent experiments, each performed in 8 replicates, determined by MTT assay.

Table 2

Synthetic yields and antiproliferative activity (nM) of α -naphthylamine-based podophyllotoxin-mimetics.

MCR product										
Ar										
										
18: ^a 14% ^b	18 ± 2	14 ± 1	27: 50%	20: 22%	21: 41%	22: 74%	23: 68%	24: 35%	25: 56%	
3 ± 0 ^c	16 ± 2	14 ± 1	6 ± 1	3 ± 0	18 ± 2	3 ± 0	3 ± 0	7 ± 2	3 ± 0	
3 ± 0 ^d			3 ± 0	3 ± 0	21 ± 1	3 ± 0	3 ± 0	13 ± 3	3 ± 0	
26: 63%			28: 34%	29: 42%	29: 42%	30: 58%	31: 42%	32: 28%	33: 33%	
2 ± 0	6 ± 1	3 ± 0	2 ± 0	7 ± 4	7 ± 4	6 ± 1	3 ± 1	3 ± 0	3 ± 0	
3 ± 1	3 ± 0	3 ± 0	3 ± 0	3 ± 0	3 ± 0	3 ± 0	3 ± 1	3 ± 0	3 ± 0	

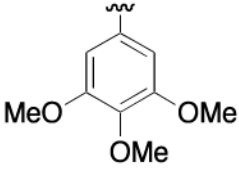
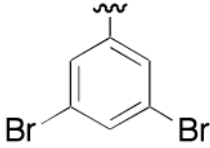
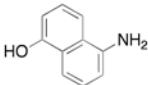
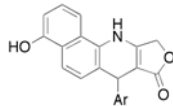
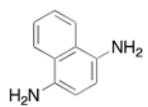
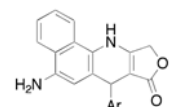
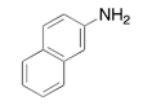
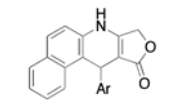
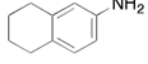
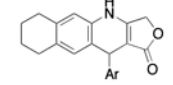
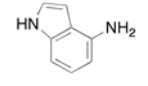
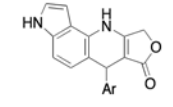
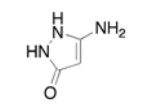
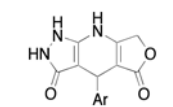
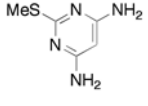
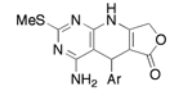
^aCompound number;

^bSynthetic yield of the MCR used to obtain this heterocycle;

^{c,d}Concentrations (nM) required to reduce the viability of HeLa (c) and MCF-7 (d) cells by 50% after 48 h of treatment with indicated compounds, relative to DMSO control; ± SD from two independent experiments, each performed in 8 replicates, determined by MTT assay.

Table 3

Further exploration of A,B-ring system substitutions in podophyllotoxin mimetics.

entry	starting amine	MCR product	synthetic yield and antiproliferative GI ₅₀ (nM)	
		Ar		
1			34 ^a : 59% ^b 3 ± 0 ^c 3 ± 0 ^d	35 : 77% 21 ± 2 23 ± 6
2			36 : 0%	37 : 66% 21 ± 0 16 ± 4
3			38 : 62% 540 ± 23 121 ± 3	39 : 78% 420 ± 180 201 ± 22
4			40 : 13% 18 ± 1 19 ± 1	41 : 31% 100 ± 5 70 ± 54
5			42 : 56% 19 ± 2 22 ± 1	43 : 39% 114 ± 0 21 ± 0
6			44 : 45% >10,000 >10,000	45 : 38% >10,000 >10,000
7			46 : 60% 125 ± 20 170 ± 25	47 : 36% 561 ± 290 1,020 ± 230

^aCompound number;^bSynthetic yield of the MCR used to obtain this heterocycle;^{c,d}Concentrations (nM) required to reduce the viability of HeLa (c) and MCF-7 (d) cells by 50% after 48 h of treatment with indicated compounds, relative to DMSO control; ± SD from two independent experiments, each performed in 8 replicates, determined by MTT assay.